Tropospheric Chemistry in the Integrated Forecasting System of ECMWF

J. Flemming[1], V. Huijnen[2], J. Arteta[3], P. Bechtold[1], A. Beljaars[1], A.-M. Blechschmidt[4], B. Josse[3], M. Diamantakis[1], R. J. Engelen[1], A. Gaudel[5], A. Inness[1], L. Jones[1], E. Katragkou[6], V. Marecal[3], V.-H. Peuch[1], A. Richter[4], M.G. Schultz[7], O. Stein[7] and A. Tsikerdekis[6]

[1] European Centre for Medium-Range Weather Forecasts, Reading, UK

[2] Royal Netherlands Meteorological Institute, De Belt, The Netherlands

[3] Météo-France, Toulouse, France

[4] Universität Bremen, Germany

[5] CNRS, Laboratoire d'Aérologie, UMR 5560, Toulouse, France

[6] Department of Meteorology and Climatology, School of Geology, Aristotle University of Thessaloniki, Greece

[7] Institute for Energy and Climate Research, Forschungszentrum Jülich, Germany

Correspondence to: J. Flemming (Johannes.Flemming@ecmwf.int)

Abstract

A representation of atmospheric chemistry has been included in the Integrated Forecasting System (IFS) of the European Centre for Medium-range Weather Forecasts (ECMWF). The new chemistry modules complement the aerosol modules of the IFS for atmospheric composition, which is named C-IFS. C-IFS for chemistry supersedes a coupled system, in which the Chemical Transport Model (CTM) Model for OZone and Related chemical Tracers 3 was two-way coupled to the IFS (IFS-MOZART). This paper contains a description of the new on-line implementation, an evaluation with observations and a comparison of the performance of C-IFS with MOZART and with a re-analysis of atmospheric composition produced by IFS-MOZART within the Monitoring Atmospheric Composition and Climate (MACC) project. The chemical mechanism of C-IFS is an extended version of the Carbon Bond 2005 (CB05) chemical mechanism as implemented in the CTM Transport Model 5 (TM5). CB05 describes tropospheric chemistry with 54 species and 126 reactions. Wet deposition and lightning nitrogen monoxide (NO) emissions are modelled in C-IFS using the detailed input of the IFS physics package. A one-year simulation by C-IFS, MOZART and the MACC re-analysis is evaluated against ozonesondes, carbon monoxide (CO) aircraft profiles, European surface observations of ozone (O_3), CO, sulphur dioxide (SO_2) and nitrogen dioxide (NO_2) as well as satellite retrievals of CO, tropospheric NO_2 and formaldehyde. Anthropogenic emissions from the MACC/CityZen (MACCity) inventory and biomass burning emissions from the Global Fire Assimilation System (GFAS) data set were used in the simulations by both C-IFS and MOZART. C-IFS (CB05) showed an improved performance with respect to MOZART for CO, upper tropospheric O_3, winter time SO_2 and was of a similar accuracy for other evaluated species. C-IFS (CB05) is about ten times more computationally efficient than IFS-MOZART.

1 Introduction

Monitoring and forecasting of global atmospheric composition are key objectives of the atmosphere service of the European Copernicus Programme. The Copernicus Atmosphere Monitoring Service (CAMS) is based on combining satellite observations of atmospheric composition with state-of-the-art atmospheric modelling (Flemming et al., 2013 and Hollingsworth et al., 2008). For that purpose, the integrated forecasting system (IFS) of the European Centre for Medium-Range Weather Forecasts (ECMWF) was extended for forecast and assimilation of atmospheric composition. Modules for aerosols (Morcrette et al., 2009,

Benedetti et al., 2009) and greenhouse gases (Engelen et al., 2009) were integrated on-line in the IFS. Because of the complexity of the chemical mechanisms for reactive gases, modules for atmospheric chemistry were not initially included in the IFS. Instead a coupled system (Flemming et al., 2009a) was developed, which couples the IFS to the Chemical Transport Model (CTM) Model for OZone and Related chemical Tracers 3 (MOZART, Kinnison et al., 2007) or Transport Model 5 (TM5, Huijnen et al., 2010) by means of the Ocean Atmosphere Sea Ice Soil coupling software (OASIS4) coupler software (Redler et al., 2010). Van Noije et al. (2014) coupled TM5 to IFS for climate applications in a similar approach. The coupled system made it possible to assimilate satellite retrievals of reactive gases with the assimilation algorithm of the IFS, which is also used for the assimilation of meteorological observations as well as for aerosol and greenhouse gases.

The coupled system IFS-MOZART has been successfully used for a re-analysis of atmospheric composition (Inness et al., 2013), pre-operational atmospheric composition forecasts (Stein et al., 2012), forecast and assimilation of the stratospheric ozone (O_3) (Flemming et al., 2011a, Lefever et al., 2014) and tropospheric carbon monoxide (CO) (Eligundi et al., 2010) and O_3 (Ordonez et al., 2010). The coupled system IFS-TM5 has been used in a case study on a period with intense biomass burning in Russia in 2010 (Huijnen et al., 2012). Nevertheless, the coupled approach has limitations such as the need for interpolation between the IFS and CTM model grids and the duplicate simulation of transport processes. Further, its computational performance is often not optimal as it can suffer from load imbalances between the coupled components.

Consequently, modules for atmospheric chemistry and related physical processes have now been integrated on-line in the IFS, thereby complementing the on-line integration strategy already pursued for aerosol and greenhouse gases in IFS. The IFS including modules for atmospheric composition is named Composition-IFS (C-IFS). C-IFS makes it possible (i) to use the detailed meteorological simulation of the IFS for the simulation of the fate of constituents (ii) to use the IFS data assimilation system to assimilate observations of atmospheric composition and (iii) to simulate feedback processes between atmospheric composition and weather. A further advantage of C-IFS is the possibility of model runs at a high horizontal and vertical resolution because of the high computational efficiency of C-IFS. C-IFS is the global model system run in pre-operational mode as part of the Monitoring

Atmospheric Composition and Climate - Interim Implementation project (MACC II and MACC III) in peraration of CAMS.

Including chemistry modules in general circulation models (GCM) to simulate interaction of stratospheric O_3 (e.g. Steil et al., 1998) and aerosols (e.g. Haywood et al., 1997) in the climate system started in the mid-1990s. Later, more comprehensive schemes for tropospheric chemistry were included in climate GCM such as ECHAM5-HAMMOZ (Pozzoli et al., 2008; Rast et al., 2014) and CAM-chem (Lamarque et al., 2012) to study short-lived greenhouse gases and the influence of climate change on air pollution (e.g. Fiore et al., 2010). In the UK Met Office's Unified Model (UM) stratospheric chemistry (Morgenstern et al., 2009) and tropospheric chemistry (O'Connor et al., 2014) can be simulated together with the GLOMAP mode aerosol scheme (Mann et al., 2010). Examples of the on-line integration of chemistry modules in global circulation models with focus on NWP are GEM-AQ (Kaminski et al., 2008), GEMS-BACH (Menard et al., 2007) and GU-WRF/Chem (Zhang et al., 2012). Savage et al. (2013) evaluate the performance of air quality forecast with the UM at the regional scale. Baklanov et al. (2014) give a comprehensive overview of on-line coupled chemistry-meteorological models for regional applications.

C-IFS is intended to run with several chemistry schemes for both the troposphere and the stratosphere in the future. Currently, only the tropospheric chemical mechanism CB05 originating from the TM5 CTM (Huijnen et al., 2010) has been thoroughly tested. For example, C-IFS (CB05) has been applied to study the HO_2 uptake on clouds and aerosols (Huijnen et al., 2014) and pollution in the Artic (Emmons et al., 2014). The tropospheric and stratospheric scheme RACMOBUS of the MOCAGE model (Bousserez et al., 2007) and the MOZART 3 chemical scheme as well as an extension of the CB05 scheme with the stratospheric chemical mechanism of the BASCOE model (Errera et al., 2008) have been technically implemented and are being scientifically tested. Only C-IFS (CB05) is the subject of this paper.

Each chemistry scheme in C-IFS consists of the specific gas phase chemical mechanism, multi-phase chemistry, the calculation of photolysis rates and upper chemical boundary conditions. Dry and wet deposition, emission injection and parameterization of lightning NO emissions as well as transport and diffusion are simulated by the same approach for all chemistry schemes. Likewise, emissions and dry deposition input data are kept the same for all configurations.

120 The purpose of this paper is to document C-IFS and to present its model performance with
121 respect to observations. Since C-IFS (CB05) replaced the current operational MACC model
122 system for reactive gases (IFS-MOZART) both in data assimilation and forecast mode, the
123 evaluation in this paper is carried out predominately with observations that are used for the
124 routine evaluation of the MACC II system. The model results are compared (i) with a
125 MOZART stand-alone simulation, which is equivalent to a IFS-MOZART simulation and (ii)
126 with the MACC re-analysis (Inness et al., 2013), which is an application of IFS-MOZART in
127 data assimilation mode. All model configurations used the same emission data. The
128 comparison demonstrates that C-IFS is ready to be used operationally.

129 The paper is structured as follows. Section 2 is a description of the C-IFS, with focus on the
130 newly implemented physical parameterizations and the chemical mechanism CB05. Section 3
131 contains the evaluation with observations of a one year simulation with C-IFS (CB05) and a
132 comparison with the results from the MOZART run and the MACC re-analysis. The paper is
133 concluded with a summary and an outlook in section 4.

134 # 2 Description of C-IFS

135 ## 2.1 Overview of C-IFS

136 The IFS consists of a spectral NWP model that applies the semi-Lagrangian (SL) semi-
137 implicit method to solve the governing dynamical equations. The simulation of the
138 hydrological cycle includes prognostic representations of cloud fraction, cloud liquid water,
139 cloud ice, rain and snow (Forbes et al., 2011). The simulations presented in this paper used
140 the IFS release CY40r1. The technical and scientific documentation of this IFS release can be
141 found at http://www.ecmwf.int/research/ifsdocs/CY40r1/index.html. Changes of the
142 operational model are documented on
143 https://software.ecmwf.int/wiki/display/IFS/Operational+changes.

144 At the start of the time step, the three-dimensional advection of the tracers mass mixing ratios
145 is simulated by the SL method as described in Temperton et al. (2001) and Hortal (2002).
146 Next, the tracers are vertically distributed by the diffusion scheme (Beljaars et al., 1998) and
147 by convective mass fluxes (Bechtold et al., 2014). The diffusion scheme also simulates the
148 injection of emissions and the loss by dry deposition (see section 2.4.1). The output of the
149 convection scheme is used to calculate NO production by lightning (see section 2.4.3).
150 Finally, the sink and source terms due to chemical conversion (see section 2.5), wet

deposition (see section 2.4.2) and prescribed surface and stratospheric boundary conditions are calculated (see section 2.5.2).

The chemical species and the related processes are represented only in grid-point space. The horizontal grid is a reduced Gaussian grid (Hortal and Simmons, 1991). C-IFS can be run at varying vertical and horizontal resolutions. The simulations presented in this paper were carried out at a T255 spectral resolution (i.e. truncation at wavenumber 255), which corresponds to a grid box size of about 80 km. The vertical discretization uses 60 levels up to the model top at 0.1 hPa (65 km) in a hybrid sigma-pressure coordinate. The vertical extent of the lowest level is about 17 m; it is 100 m at about 300m above ground, 400-600 m in the middle troposphere and about 800 m at about 10 km height.

The modus operandi of C-IFS is one of a forecast model in a NWP framework. The simulations of C-IFS are a sequence of daily forecasts over a period of several days. Each forecast is initialised by the ECMWF's operational analysis for the meteorological fields and by the 3D chemistry fields from the previous forecast ("forecast mode"). Continuous simulations over longer periods are carried out in "relaxation mode". In relaxation mode the meteorological fields are relaxed to the fields of a meteorological re-analysis, such as ERA-Interim, during the run (Jung et al., 2008) to ensure realistic and consistent meteorological fields.

2.2 Transport

The transport by advection, convection and turbulent diffusion of the chemical tracers uses the same algorithms as developed for the transport of water vapour in the NWP applications of IFS. The advection is simulated with a three-dimensional semi-Lagrangian advection scheme, which applies a quasi-montonic cubic interpolation of the departure values. Since the semi-Lagrangian advection does not formally conserve mass a global mass fixer is applied. The effect of different global mass fixers is discussed in Diamantakis and Flemming (2014) and Flemming and Huijnen (2011b). A proportional mass was used for the runs presented in this paper because of the overall best balance between the results and computational cost.

The vertical turbulent transport in the boundary layer is represented by a first order K-diffusion closure. The surface emissions are injected as lower boundary flux in the diffusion scheme. The lower boundary flux condition also accounts for the dry deposition flux based on the projected surface mass mixing ratio in an implicit way. The vertical transport by

convection is simulated as part of the cumulus convection. It applies a bulk mass flux scheme which was originally described in Tiedtke (1989). The scheme considers deep, shallow and mid-level convection. Clouds are represented by a single pair of entraining/detraining plumes which determine the updraught and downdraught mass fluxes. (http://old.ecmwf.int/research/ifsdocs/CY40r1/ in Physical Processes, Chapter 6, pp 73-90). Highly soluble species such as nitr/ic acid (HNO_3), hydrogen peroxide (H_2O_2) and aerosol precursors are assumed to be scavenged in the convective rain droplets and are therefore excluded from the convective mass transfer.

The operator splitting between the transport and the sink and source terms follows the implementation for water vapour (Beljaars et al., 2004). Advection, diffusion and convection are simulated sequentially. The sink and source processes are simulated in parallel using an intermediate update of the mass mixing ratios with all transport tendencies. At the end of the time step tendencies from transport and sink and source terms are added together for the final update the concentration fields. Resulting negative mass mixing ratios are corrected at this point by setting the updated mass mixing ratio to a "chemical zero" of 1.0e-25 kg/kg. For the majority of the species the contribution of the negative fixer was below 0.1% of the dominating source or sink term. The contribution was of the order of 1% for nitrogen species such as NO, N_2O_5 as well as up to 3% for highly soluble species such HNO_3, HO_2, NO_3_A. Large gradients of NO_x at the terminator in the stratosphere as well as intensive wet deposition were the reasons for the increased occurrence of projected negative concentrations.

2.3 Emissions for 2008

The anthropogenic surface emissions were given by the MACCity inventory (Granier et al., 2011) and aircraft NO emissions of a total of ~0.8 Tg N/yr were applied (Lamarque et al, 2010). Natural emissions from soils and oceans were taken from the Precursors of Ozone and their Effects in the Troposphere (POET) database for 2000 (Granier et al., 2005; Olivier et al., 2003). The biogenic emissions were simulated off-line by the MEGAN2.1 model (Guenther et al., 2006). The anthropogenic and natural emissions were used as monthly means without accounting for the diurnal cycle. Daily Biomass burning emissions were produced by the Global Fire Assimilation System (GFAS) version 1, which is based on satellite retrievals of fire radiative power (Kaiser et al., 2012). The actual emission totals used in the T255 simulation for 2008 from anthropogenic, biogenic sources and biomass burning as well as lighting NO are given in Table 1.

2.4 Physical parameterizations of sources and sinks

2.4.1 Dry deposition

Dry deposition is an important removal mechanism at the surface in the absence of precipitation. It depends on the diffusion close to the earth surface, the properties of the constituent and on the characteristics of the surface, in particular the type and state of the vegetation and the presence of intercepted rain water. Dry deposition plays an important role in the biogeochemical cycles of nitrogen and sulphur, and it is a major loss process of tropospheric O_3. Modelling the dry deposition fluxes in C-IFS is based on a resistance model (Wesely et al., 1989), which differentiates the aerodynamic, the quasi-laminar and the canopy or surface resistance. The inverse of the total resistance is equivalent to a dry deposition velocity V_D.

The dry deposition flux F_D at the model surface is calculated based on the dry deposition velocity V_D, the mass mixing ratio X_s and air density ρ_s at the lowest model level *s,* in the following way:

$$F_D = V_D \, X_S \, \rho_S$$

The calculation of the loss by dry deposition has to account for the implicit character of the dry deposition flux since it depends on the mass mixing ratio X_s.

The dry deposition velocities were calculated as monthly mean values from a one-year simulation using the approach described in Michou et al. (2004). It used meteorological and surface input data such as wind speed, temperature, surface roughness and soil wetness from the ERA-interim data set. At the surface the scheme makes a distinction between uptake resistances for vegetation, bare soil, water, snow and ice. The surface and vegetation resistances for the different species are calculated using the stomatal resistance of water vapour. The stomatal resistance for water vapour is calculated depending on the leaf area index, radiation and the soil wetness at the uppermost surface layer. Together with the cuticlular and mesophyllic resistances this is combined into the leaf resistance according to Wesely et al. (1989) using season and surface type specific parameters as referenced in Seinfeld and Pandis (1998).

Dry deposition velocities have higher values during the day because of lower aerodynamic resistance and canopy resistance. Zhang et al. (2003) reported that averaged observed O_3 and sulphur dioxide (SO_2) dry deposition velocities can be up to 4 times higher at day time than at

night time. As this important variation is not captured with the monthly-mean dry deposition values, a +/- 50% variation is imposed on all dry deposition values based on the cosine of the solar zenith angle. This modulation tends to decrease dry deposition for species with a night time maximum at the lowest model level and it increases dry deposition of O_3.

Table A4 (supplement) contains annual total loss by dry deposition and expressed as a life-time estimate by dividing by tropospheric burden for a simulation using monthly dry deposition values for 2008. Dry deposition was most effective for many species in particular SO_2 and ammonia (NH_3) as the respective lifetimes were one day to one week. For tropospheric O_3 the respective globally averaged time scale is about 3 months. Because dry deposition occurs mainly over ice-free land surfaces the corresponding time scale is at least three times shorter in these areas.

2.4.2 Wet Deposition

Wet deposition is the transport and removal of soluble or scavenged constituents by precipitation. It includes the following processes:

- In-cloud scavenging and removal by rain and snow (rain out)
- Release by evaporation of rain and snow
- Below cloud scavenging by precipitation falling through without formation of precipitation (wash out)

It is important to take the sub-grid scale of cloud and precipitation-formation into account for the simulation of wet deposition. The IFS cloud scheme provides information on the cloud and the precipitation fraction for each grid box. It uses a random overlap assumption (Jakob and Klein, 2000) to derive cloud and precipitation area fraction. The same method has been used by Neu and Prather (2012), who demonstrated the importance of the overlap assumption for the simulation of the wet deposition. The precipitation fluxes for the simulation of wet removal in C-IFS were scaled to be valid over the precipitation fraction of the respective grid-box. The loss of tracer by rain-out and wash-out was limited to the area of the grid box covered by precipitation. Likewise, the cloud water and ice content is scaled to the respective cloud area fraction. If the sub-grid scale distribution was not considered in this way, wet deposition was lower for highly soluble species such as HNO_3 because the species is only removed from the cloudy or rainy grid box fraction. For species with low solubility the wet deposition loss was slightly decreased because of the decrease in effective cloud and rain water.

Even if wet deposition removes tracer mass only in the precipitation area, the mass mixing ratio representing the entire grid box is changed accordingly after each model time step. This is equivalent with the assumption that there is instantaneous mixing within the grid-box at the time scale of the model time step. As discussed in Huijnen et al. (2014), this assumption may lead to an overestimation of the simulated tracer loss.

The module for wet deposition in C-IFS is based on the Harvard wet deposition scheme (Jacob et al., 2000 and Liu et al., 2001). In contrast to Jacob et al. (2000), tracers scavenged in wet convective updrafts are not removed as part of the convection scheme. Nevertheless, the fraction of highly soluble tracers in cloud condensate is simulated to limit the amount of tracers lifted upwards as only the gas phase fraction is transported by the mass flux. The removal by convective precipitation is simulated in the same way as for large-scale precipitation in the wet deposition routine.

The input fields to the wet deposition routine are the following prognostic variables, calculated by the IFS cloud scheme (Forbes et al., 2011): total cloud and ice water content, grid-scale rain- and snow water content and cloud and grid-scale precipitation fraction as well as the derived fluxes for convective and grid-scale precipitation fluxes at the grid cell interfaces. For convective precipitation a precipitation fraction of 0.05 is assumed and the convective rain and snow water content is calculated assuming a droplet fall speed of 5 m/s.

Wash-out, evaporation and rain-out are calculated after each other for large-scale and convective precipitation. The amount of trace gas dissolved in cloud droplets is calculated using Henrys-law-equilibrium or assuming that 70% of aerosol precursors such as sulphate (SO_4), NH_3 and nitrate (NO_3) is dissolved in the droplet. The effective Henry coefficient for SO_2, which accounts for the dissociation of SO_2, is calculated following Seinfeld and Pandis (1998, p. 350). The other Henry's law coefficients are taken from the compilation by Sander (1999) (www.henrys-law.org, Table A1 in the supplement).

The loss by rain out is determined by the precipitation formation rate. The retention coefficient R, which accounts for the retention of dissolved gas in the liquid cloud condensate as it is converted to precipitation, is one for all species in warm clouds ($T > 268$ K). For mixed clouds ($T < 268$ K) R is 0.02 for all species but 1.0 for HNO_3 and 0.6 for H_2O_2 (von Blohn, 2011). In ice clouds only H_2O_2 (Lawrence and Crutzen, 1998) and HNO_3 are scavenged.

Partial evaporation of the precipitation fluxes leads to the release of 50% of the resolved tracer and 100% in the case of total evaporation (Jacobs et al., 2000). Wash-out is either mass-transfer or Henry-equilibrium limited. HNO_3, aerosol precursors and other highly soluble gases are washed out using a first order wash-out rate of 0.1 mm^{-1} (Levine and Schwartz, 1982) to account for the mass transfer . For less soluble gases the resolved fraction in the rain water is calculated assuming Henry equilibrium in the evaporated precipitation.

Table A5 (supplement) contains total loss by wet deposition and expressed as time scale in days based on the tropospheric burden. For aerosol precursors nitrate, sulphate and ammonium, HNO_3 and H_2O_2 wet deposition is the most important loss process with respective timescales of 2–4 days.

2.4.3 NO emissions from lightning

NO emissions from lightning are a considerable contribution to the global atmospheric NO_x budget. Estimates of the global annual source vary between 2–8 TgN/yr (Schumann and Huntrieser, 2007). 5 TgN/yr (10.7 TgNO/yr) is the most commonly assumed value for global CTMs which is about 6-7 times the value of NO emissions from aircraft (Gauss et al., 2006) or 17% of the total anthropogenic emissions. NO emissions from lightning play an important role in the chemistry of the atmosphere because they are released in the rather clean air of the free troposphere, where they can influence the O_3 budget and hence the OH-HO_2 partitioning (DeCaria et al., 2005) .

The parameterization of the lightning NO production in C-IFS consist of estimates of (i) the flash rate density, (ii) the flash energy release and (iii) the vertical emission profile for each model grid column. The estimate of the flash-rate density is based on parameters of the convection scheme. The C-IFS has two options to simulate the flash-rate densities using the following input parameters: (i) convective cloud height (Price and Rind, 1992) or (ii) convective precipitation (Meijer et al., 2001).

The parameterizations distinguish between land and ocean points by assuming about 5-10 times higher flash rates over land. Additional checks on cloud base height, cloud extent and temperature are implemented to select only clouds that are likely to generate lightning strokes. The coefficients of the two parameterizations were derived from field studies and depend on the model resolution. With the current implementation of C-IFS (T255L60), the global flash rates were 26 and 43 flashes per seconds for the schemes by Price and Rind (1992) and Meijer

et al. (2001), respectively. It seemed therefore necessary to scale the coefficients to get a flash rate in the range of the observed values of about 40-50 flashes per second derived from observations of the Optical Transient Detector (OTD) and the Lightning Imaging Sensor (LIS) (Cecil et al., 2012). Figure 1 shows the annual flash rate density simulated by the two parameterisations together with observations from the LIS/OTD data set. The two approaches show the main flash activity in the tropics but there were differences in the distributions over land and sea. The smaller land-sea differences of Meijer et al. (2001) agreed better with the observations. The observed maximum over Central Africa was well reproduced by both parameterizations but the schemes produce an exaggerated maximum over tropical South America. The lightning activity over the United States was underestimated by both parameterisations. The parameterization by Meijer et al. (2001) has been used for the C-IFS runs presented in this paper.

Cloud to ground (CG) and cloud to cloud (CC) flashes are assumed to release a different amount of energy, which is proportional to the NO release. Price et al. (1997) suggest that the energy release of CG is 10 times higher. However, more recent studies suggest a similar value for CG and CC energy release based on aircraft observations and model studies (Ott et al., 2010), which is followed in C-IFS. In C-IFS, CG and CC fractions are calculated using the approach by Price and Rind (1993), which is based on a 4th order function of cloud height above freezing level.

The vertical distribution of the NO release is of importance for its impact on atmospheric chemistry. Many CTMs use the suggestion of Pickering et al. (1998) of a C-shape profile, which peaks at the surface and in the upper troposphere. Ott et al. (2010) suggest a “backward C-shape” profile which locates most of the emission in the middle of the troposphere. The vertical distribution can be simulated by C-IFS (i) according to Ott et al. (2010) or (ii) as a C-shape profile following Huijnen et al. (2010). The approach by Ott et al. (2010) is used in the simulation presented here. As lightning NO emissions occur mostly in situations with strong convective transport, differences in the injection profile had little impact.

As the lightning emissions depend on the convective activity they change at different resolutions or after changes to the convection scheme. The C-IFS lightning emissions, using the parameterization of Meijer et al. (2001) based on convective precipitation, were 4.9 TgN/yr at T159 resolution and 5.7 Tg N/yr at T255 resolution.

2.5 CB05 chemistry scheme

2.5.1 Gas-phase chemistry

The chemical mechanism is a modified version of the Carbon Bond mechanism 5 (CB05, Yarwood et al., 2005), which is originally based on the work of Gery et al. (1989) with added reactions from Zaveri and Peters (1999) and from Houweling et al. (1998) for isoprene. The CB05 scheme adopts a lumping approach for organic species by defining a separate tracer species for specific types of functional groups. The speciation of the explicit species into lumped species follows the recommendations given in Yarwood et al. (2005). The CB05 scheme used in C-IFS has been further extended in the following way: An explicit treatment of methanol (CH_3OH), ethane (C_2H_6), propane (C_3H_8), propene (C_3H_6) and acetone (CH_3COCH_3) has been introduced as described in Williams et al., (2013). The isoprene oxidation has been modified motivated by Archibald et al. (2010). Higher C3 peroxy-radicals formed during the oxidation of C_3H_6 and C_3H_8 were included following Emmons et al. (2010).

The CB05 scheme is supplemented with chemical reactions for the oxidation of SO_2, di-methyl sulphide (DMS), methyl sulphonic acid (MSA) and NH_3, as outlined in Huijnen et al. (2014). For the oxidation of DMS, the approach of Chin et al. (1996) is adopted. Table A1 (supplement) gives a comprehensive list of the trace gases included in the chemical scheme.

The reaction rates have been updated according to the recommendations given in either Sander et al. (2011) or Atkinson et al. (2004, 2006). The oxidation of CO by the hydroxyl radical (OH) implicitly accounts for the formation and subsequent decomposition of the intermediate species HOCO as outlined in Sander et al. (2006). For lumped species, e.g. ALD2, the reaction rate is determined by an average of the rates of reaction for the most abundant species, e.g. C2 and C3 aldehydes, in that group. An overview of all gas-phase reactions and reaction rates as applied in this version of C-IFS can be found in Table A2 (supplement).

For the loss of trace gases by heterogeneous oxidation processes, the model explicitly accounts for the oxidation of SO_2 in cloud through aqueous phase reactions with H_2O_2 and O_3, depending on the acidity of the solution. The pH is computed from the SO4, MSA, HNO3, NO3_A, NH3 and NH4 concentrations, as well as from a climatological CO2 value. The pH, in combination with the Henry coefficient, defines the fraction of sulphate residing in the

aqueous phase, compared to the gas phase concentration (Dentener and Crutzen, 1993) The heterogeneous conversion of N_2O_5 into HNO_3 on cloud droplets and aerosol particles is applied with a reaction probability (γ) set to 0.02 (Evans and Jacob, 2005). The surface area density is computed based on a climatological aerosol size distribution function, applied to the SO_4, MSA and NO3_A aerosol, as well as to clouds assuming a droplet size of 8 μm.

2.5.2 Photolysis rates

For the calculation of photo-dissociation rates an on-line parameterization for the derivation of actinic fluxes is used (Williams et al., 2012, 2006). It applies a Modified Band Approach (MBA) which is an updated version of the work by Landgraf and Crutzen (1998), tailored and optimized for use in tropospheric CTMs. The approach uses 7 absorption bands across the spectral range 202 – 695 nm. At instances of large solar zenith angles (71-85°) a different set of band intervals is used. In the MBA the radiative transfer calculation using the absorption and scattering components introduced by gases, aerosols and clouds is computed on-line for each of 7 pre-defined band intervals based on the 2-stream solver of Zdunkowski et al. (1980).

The optical depth of clouds is calculated based on a parameterization available in IFS (Slingo, 1989 and Fu et al., 1996) for the cloud optical thickness at 550 nm. For the simulation of the impact of aerosols on the photolysis rates a climatological field for aerosols is used, as detailed in Williams et al. (2012). There is also an option to use the MACC aerosol fields.

In total 20 photolysis rates are included in the scheme, as given in Table A3 (supplement). The explicit nature of the MBA implies a good flexibility in terms of updating molecular absorption properties (cross sections and quantum yields) and the addition of new photolysis rates into the model.

2.5.3 The chemical solver

The chemical solver used in C-IFS (CB05) is an Euler Backward Iterative (EBI) solver (Hertel et al., 1996). This solver has been originally designed for use with the CBM4 mechanism of Gery et al. (1989). The chemical time step is 22.5 min, which is half of the dynamical model time step of 45 min at T255 resolution. Eight, four or one iterations are carried out for fast-, medium- and slow-reacting chemical species to obtain a solution. The number of iterations is doubled in the lowest four models levels, where the perturbations due to emissions can be large.

2.5.4 *Stratospheric boundary conditions*

The modified CB05 chemical mechanism includes no halogenated species and no photolytic destruction below 202 nm and is therefore not suited for the description of stratospheric chemistry. Thus realistic upper boundary conditions for the longer-lived gases such as O_3, methane (CH_4), and HNO_3 are needed to capture the influence of stratospheric intrusions on the composition of the upper troposphere.

Stratospheric O_3 chemistry in C-IFS (CB05) is parameterized by the Cariolle scheme (Cariolle and Teyssèdre, 2007). Chemical tendencies for stratospheric and tropospheric O_3 are merged at an empirical interface of the diagnosed tropopause height in IFS. Additionally, stratospheric O_3 in C-IFS can be nudged to O_3 analyses of either the MACC re-analysis (Inness et al., 2013) or ERA interim (Dee et al., 2011). The tropopause height in IFS is diagnosed either from the gradient in humidity or the vertical temperature gradient.

Stratospheric HNO_3 at 10 hPa is controlled by a climatology of HNO_3 and O_3 observations from the Microwave Limb Sounder (MLS) aboard the Upper Atmosphere Research satellite (UARS). HNO_3 is set to according to the observed HNO_3 - O_3 ratio and the simulated O_3 concentrations. Further, stratospheric CH_4 is constrained by a climatology based on observations of the Halogen Occultation Experiment instrument (Grooß and Russel, 2005), at 45hPa and at 90 hPa in the extra-tropics, which implicitly accounts for the stratospheric chemical loss of CH_4 by OH, chlorine (Cl) and oxygen (O^1D) radicals. It should be noted that also the surface concentrations of CH_4 are fixed in this configuration of the model.

2.5.5 *Gas-aerosol partitioning*

Gas-aerosol partitioning is calculated using the Equilibrium Simplified Aerosol Model (EQSAM, Metzger et al., 2002a, 2002b). The scheme has been simplified so that only the partitioning between HNO_3 and the nitrate aerosol (NO^-_3) and between NH_3 and the ammonium aerosol (NH^+_4) is calculated. SO^{2-}_4 is assumed to remain completely in the aerosol phase because of its very low vapour pressure. The assumptions of the equilibrium model are that (i) aerosols are internally mixed and obey thermodynamic gas/aerosol equilibrium and that (ii) the water activity of an aqueous aerosol particle is equal to the ambient relative humidity (RH). Furthermore, the aerosol water mainly depends on the aerosol mass and the type of the solute, so that parameterizations of single solute molalities and activity coefficients can be defined, depending only on the type of the solute and RH. The advantage of using such parameterizations is that the entire aerosol equilibrium composition

can be solved analytically. For atmospheric aerosols in thermodynamic equilibrium with the ambient RH, the following reactions are considered in C-IFS. The subscripts g, s and aq denote gas, solid and aqueous phase, respectively:

$(NH_3)_g + (HNO_3)_g \leftrightarrow (NH_4NO_3)_s$

$(NH_4NO_3)_s + (H_2O)_g \leftrightarrow (NH_4NO_3)_{aq} + (H_2O)_{aq}$

$(NH_4NO_3)_{aq} + (H_2O)_g \leftrightarrow (NH^+_4)_{aq} + (NO^-_3)_{aq} + (H_2O)_{aq}$

2.6 Model budget diagnostics

C-IFS computes global diagnostics for every time step to study the contribution of different processes on the global budget. The basic outputs are the total and tropospheric tracer mass, the global integral of the total surface emissions, integrated wet and dry deposition fluxes, chemical conversion as well as elevated atmospheric emissions and the contributions of prescribed upper and lower vertical boundary conditions for CH_4 and HNO_3. A time-invariant pressure-based tropopause definition, which varies with latitude, is used to calculate the tropospheric mass. To monitor the numerical integrity of the scheme, the contributions of the corrections to ensure positiveness and global mass conservation are calculated. Optionally, more detailed diagnostics can be requested that includes photolytic loss and the loss by OH for the tropics and extra-tropics.

A detailed analysis of the global chemistry budget is beyond the scope of this paper. Only a number of key terms for CO, O_3 and CH_4 is summarized here. They are compared with values from the "Atmospheric Composition Change: the European Network of Excellence" (ACCENT) model inter-comparisons of chemistry models by Stevenson et al. (2006) for tropospheric O_3 and by Shindell et al. (2006) for CO. A more recent inter-comparison was carried out within the Atmospheric Chemistry and Climate Model Intercomparison Project (ACCMIP) (Lamarque et al., 2013). The ACCMIP values have been taken from Young et al. (2013) for tropospheric O_3 and from Voulgarakis et al. (2013) for CH_4. It should be noted that the values from these inter-comparisons are valid for present-day conditions but not specifically for 2008. A further source of the differences is the height of the tropopause assumed in the calculations. Overall, the comparison showed that the C-IFS (CB05) is well within the range of the two multi model ensembles.

The annual mean of C-IFS tropospheric O_3 burden was 390 Tg. The values are at the upper end of the range simulated by the ACCENT (344 ± 39 Tg) and the ACCMIP (337 ± 23 Tg)

models. The same holds for the loss by dry deposition, which was 1155 Tg/yr for C-IFS, 1003 ± 200 Tg/yr for ACCENT and in the range 687-1350 Tg/yr for ACCMIP. The tropospheric chemical O_3 production of C-IFS was 4608 Tg/yr and loss 4144 Tg/yr, which is for both values at the lower end of the range reported for the production (5110 ± 606 Tg/yr) and loss (4668 ± 727 Tg/yr) for the ACCENT models. The comparatively simple treatment of volatile organic compounds in CB05 could be an explanation for the low O_3 production and loss terms. Stratospheric inflow in C-IFS, estimated as the residue from the remaining terms was 691 Tg and the corresponding value from the ACCENT multi-model mean is 552 ± 168 Tg.

The annual mean total CO burden in C-IFS was 361 Tg, which is slightly larger than the ACCENT mean (345 Tg, 248-427 Tg). The total CO emissions in 2008 were 1008 Tg which is in-line with the number used in ACCENT (1077 Tg/yr) but lower than the estimate (1550 Tg/yr) of the Third Assessment Report (Prather et al. 2001) of the Intergovernmental Panel on Climate Change (IPCC), which also takes into account results from inverse modelling studies. The tropospheric chemical CO production was 1434 Tg/yr, which is very close to the ACCENT multi-mean of 1505 +/- 236 Tg/yr. The chemical CO loss in C-IFS was 2423 Tg and the loss by dry deposition 24 Tg.

The annual mean CH_4 total and tropospheric burdens of C-IFS (CB05) are 4874 and 4271 Tg/yr, respectively. The global chemical CH_4 loss by OH was 467 Tg/yr. Following Stevenson et al. (2006), this leads to a global CH_4 lifetime estimate of 9.1 yr. This value is within the ACCMIP range of 9.8±1.6 yr but lower than an observation-based 11.2±1.3 yr estimate by Prather et al. (2012). CH_4 emissions were substituted by prescribed monthly zonal-mean surface concentrations to avoid the long-spin up needed by a direct modelling of the CH_4 surface fluxes. The CH_4 surface concentrations were derived from a latitudinal interpolation of observations from the stations South Pole, Cape Grim, Mauna Loa, Mace Head, Barrow and Alert as discussed in Banda et al. (2015). The resulting CH_4 flux was 488 Tg/yr, which is of similar size as the sum of current estimates of the total CH_4 emissions of 500 - 580 Tg/yr and the loss by soils of 30-40 Tg/yr (Forth Assessment Report by IPCC< http://www.ipcc.ch/publications_and_data/ar4/wg1/en/ch7s7-4-1.html#ar4top).

3 Evaluation with observations and comparison with the coupled system IFS-MOZART

The main motivation for the development of C-IFS is forecasting and assimilation of atmospheric composition as part of the CAMS. Hence, the purpose of this evaluation is to show how C-IFS (CB05) performs relative to the coupled CTM MOZART-3 (Kinnison et al., 2007), which has been running in the coupled system IFS-MOZART in pre-operational mode since 2007. C-IFS will replace the coupled system in the next update of the CAMS system. The evaluation focuses on species which are relevant to global air pollution such as tropospheric O_3, CO, nitrogen doxide (NO_2), SO_2 and formaldehyde (HCHO). The MACC re-analysis (Inness et al., 2013), which is an application of IFS-MOZART with assimilation of observations of atmospheric composition, has been included in the evaluation as a benchmark.

The MACC re-analysis (REAN) and the corresponding MOZART (MOZ) stand-alone run have already been evaluated with observations by Inness et al. (2013). Further, the MACC-II sub-project on validation has compiled a comprehensive report assessing REAN (MACC, 2013). REAN has been further evaluated with surface observations in Europe and North-America for O_3 by Im et al. (2014). C-IFS (CB05) has been already evaluated with a special focus on hydroperoxyl (HO_2) in relation to CO in Huijnen et al. (2014). The performance of an earlier version of C-IFS (CB05) in the Arctic was evaluated and inter-compared with CTMs of the POLARCAT model intercomparison Project (POLMIP) by Monks et al. (2014) for CO and Arnold et al. (2014) for reactive nitrogen. The POLMIP inter-comparisons show that C-IFS (CB05) performs within the range of state-of-the-art CTMs.

3.1 Summary of model runs setup

C-IFS (CB05) was run from 1 January to 31 December 2008 with a spin up starting 1 July 2007 at a T255 resolution (80 km x 80 km) with 60 model levels in monthly chunks. The meteorological simulation was relaxed to dynamical fields of the MACC re-analysis (see section 2.1). Likewise stratospheric O_3 above the tropopause was nudged to the MACC re-analysis.

MOZ is a run with the MOZART CTM at 1.1°×1.1° (120 x 120 km) horizontal resolution using the 60 vertical levels of C-IFS. The setup of the MOZART model and the applied emissions and dry deposition velocities were the same in MOZ and REAN. The most important difference between MOZ and REAN is the assimilation of satellite retrieval of atmospheric composition in REAN. Further, REAN was produced with the coupled system

IFS-MOZART whereas MOZ is a stand-alone driven by the meteorological fields of REAN. The latter is equivalent to a simulation of IFS-MOZART without data assimilation of atmospheric composition. The assimilated retrievals were CO and O_3 total columns, stratospheric O_3 profiles and tropospheric NO_2 columns. No observations of atmospheric composition have been feed in to the MOZ run. No observational information has been used to improve the tropospheric simulation of the C-IFS run. Another difference between MOZ and REAN is that the IFS diffusion and convection scheme, as used in C-IFS, controls the vertical transport in REAN whereas MOZART's generic schemes were used in the MOZ run.

MOZ, REAN and C-IFS used the same anthropogenic emissions (MACCity), biogenic emissions (MEGAN 2.1 Guenther et al., 2006, http://acd.ucar.edu/~guenther/MEGAN/MEGAN.htm) and natural emissions from the POET project. The biomass burning emissions for MOZ and REAN came from the Global Fire Emission Data version 3 inventory which was redistributed according to Fire Radiative Power observations used in GFAS. Hence, the average biomass burning emissions used by MOZART (MOZ and REAN) agree well with the GFAS emissions used by C-IFS, but they are not identical in temporal and spatial variability.

3.2 Observations

The runs (C-IFS, MOZ, REAN) were evaluated with O_3 observations from ozonesondes and O_3 and CO aircraft profiles from the Measurement of Ozone, Water Vapour, Carbon Monoxide and Nitrogen Oxides by Airbus in-service Aircraft (MOZAIC) program. Simulated surface O_3, CO, NO_2 and SO_2 fields were compared against Global Atmospheric Watch (GAW) surface observations and additionally O_3 against observations from the of the European Monitoring and Evaluation Programme (EMEP) and the European air quality database (AirBase). The global distributions of tropospheric NO_2 and HCHO were evaluated with retrievals of tropospheric columns from Global Ozone Monitoring Experiment 2 (GOME-2). Measurements Of Pollution In The Troposphere (MOPITT) retrievals were used for the validation of the global CO total column fields.

3.2.1 In-situ observations

The ozonesondes were obtained from the World Ozone and Ultraviolet Radiation Data Centre (WOUDC) and from the ECWMF Meteorological Archive and Retrieval System. The observation error of the sondes is about ±5% in the range between 200 and 10 hPa and -7 -

17% below 200 hPa (Beekmann et al., 1994, Komhyr et al., 1995 and Steinbrecht et al., 1996). The number of soundings varied for the different stations. Typically, the sondes are launched once a week but in certain periods such as during O_3 hole conditions soundings are more frequent. Sonde launches were carried out mostly between 9 and 12 hours local time. The global distribution of the launch sites is even enough to allow meaningful averages over larger areas such North-America, Europe, the Tropics, the Artic and Antarctica. Table 2 contains a list of the ozonesondes used in this study. Tilmes et al. (2012) suggest a further refinement of the North-America region into Canada, Eastern and Western United States as well of the Tropics into Atlantic/Africa, equatorial Americas and Eastern Indian Ocean/Western Pacific based on the inter-comparison of ozone sonde observation for the 1994-2010 period. The results will be discussed also for the sub-regions and figures will be presented in the supplement.

The MOZAIC program (Marenco et al., 1998 and Nédélec et al., 2003) provides profiles of various trace gases taken during commercial aircraft ascents and descents at specific airports. MOZAIC CO data have an accuracy of ± 5 ppbv, a precision of ± 5%, and a detection limit of 10 ppbv (Nédélec et al., 2003). Since the aircraft carrying the MOZAIC unit were based in Frankfurt, the majority of the CO profiles (837 in 2008) were observed at this airport. A further 10 of the 28 airports with observations in 2008 had a sufficient number of profiles: Windhoek (323), Caracas (129), Hyderabad (125) and London-Gatwick (83) as well as the North-American airports Atlanta (104), Portland (69), Philadelphia (65), Vancouver (56), Toronto (46) and Dallas (43). The North-American airports were considered to be close enough to make a spatial average meaningful. Because of the varying data availability the North-American mean is dominated by the airports in the Eastern United States.

Apart from Frankfurt, typically 2 profiles (takeoff and landing) are taken within 2-3 hours or with a longer gap in the case of an overnight stay. At Frankfurt there were 2-6 profiles available each day, mostly in the morning and the later afternoon to the evening. At the other airports the typical observation times were 6 & 18 UTC for Windhoek (+/- 0 h local time), 19 and 21 UTC for Hyderabad (+ 4 h local time), 20 and 22 UTC for Caracas (-6 h), 4 and 22 for London (+/- 0 h) and 19 and 22 (- 5/6 h) for the North American airports. This means that most of the observations were taken between the late evening and early morning hours, i.e. at a time of increased stability and large CO vertical gradients close to the surface. Only the observations at Caracas (afternoon) and to some extent in Frankfurt represent a more mixed

day-time boundary layer. The modelled column profile was obtained at the middle between start and end time of the profile observation and no consideration was given to the horizontal movement of the aircraft. The model columns were interpolated in time between two subsequent output time steps.

The global atmospheric watch (GAW) program of the World Meteorological Organization is a network for mainly surface based observations (WMO, 2007). The data were retrieved from the World Data Centre for Greenhouse Gases [http://ds.data.jma.go.jp/gmd/wdcgg/]. The GAW observations represent the global background away from the main polluted areas. Often, the GAW observation sites are located on mountains, which makes it necessary to select a model level different from the lowest model level for a sound comparison with the model. In this study the procedure described in Flemming et al. (2009b) is applied to determine the model level, which is based on the difference between a high resolution orography and the actual station height. The data coverage for CO and O_3 was global, whereas for SO_2 and NO_2 only a few observations in Europe were available at the data repository.

The Airbase and EMEP databases host operational air quality observations from different national European networks. All EMEP stations are located in rural areas, while Airbase stations are designed to monitor local pollution. Many AirBase observations may therefore not be representative of a global model with a horizontal resolution of 80 km. However, stations of rural regime may capture the larger scale signal in particular for O_3, which is spatially well correlated (Flemming et al., 2005). The EMEP observations and the rural Airbase O_3 observations were used for the evaluation over Europe.

3.2.2 Satellite retrievals

Satellite retrievals of atmospheric composition are more widely used to evaluate model results. Satellite data provide good horizontal coverage but have limitation with respect to the vertical resolution and signal from the lowest atmospheric levels. Further, satellite observations are only possible at the specific overpass time, and they can be disturbed by the presence of clouds and surface properties. Depending on the instrument type global coverage is achieved in several days.

Day-time CO total column retrievals from MOPITT, version 6 (Deeter et al., 2013b) and retrievals of tropospheric columns of NO_2 (IUP-UB v0.7, Richter et al., 2005) and of HCHO

649 (IUP-UB v1.0; Wittrock et al., 2006) from GOME-2 (Callies et al., 2000) have been used for
650 the evaluation. The retrievals were averaged to monthly means values to reduce the random
651 retrieval error.

652 MOPITT is a multispectral thermal infrared (TIR) / near infrared (NIR) instrument onboard
653 the TERRA satellite with a pixel resolution of 22 km. TERRA's local equatorial crossing time
654 is approximately 10:30 a.m. The MOPITT CO level 2 pixels were binned within 1x1° within
655 each month. Deeter et al. (2013a) report a bias of about +0.08e^{18} molec/cm^2 and a standard
656 deviation (SD) of the error of 0.19e^{18} molec/cm^2 for the TIR/NIR product version 5. This is
657 equivalent to a bias of about 4 % and a SD of 10% respectively assuming typical observations
658 of 2.0 e^{18} molec/cm^2. For the calculation of the simulated CO total column the a-priori profile
659 in combination with the averaging kernels (AK) of the retrievals were applied. They have the
660 largest values between 300 and 800 hPa. The AK have been applied to ensure that the
661 difference between retrieval and AK-weighted model column is independent of the a-priori
662 CO profiles used in the retrieval.. One should note however, that the AK-weighted column is
663 not equivalent to the modelled atmospheric CO burden anymore..

664

665 GOME-2 is a ultra violet - visibile (UV-VIS) and NIR sensor designed to provide global
666 observations of atmospheric trace gases. GOME-2 flies in a sun-synchronous orbit with an
667 equator crossing time of 09:30 LT in descending mode and has a footprint of 40 x 80 km.
668 Here, tropospheric vertcial columns of NO_2 and HCHO have been computed using a three
669 step approach. First, the Differential Optical Absorption Spectroscopy (DOAS; Platt, 1994)
670 method is applied to measured spectra which yields the total slant column. The DOAS
671 method is applied in a 425–497 nm wavelength window (Richter et al., 2011) for NO_2. and
672 between 337 and 353 nm for HCHO (Vrekoussis et al., 2010). Second, the reference sector
673 approach is applied to total slant columns for stratospheric correction. In a last step,
674 tropospheric slant columns are converted to tropospheric vertical columns by applying an air
675 mass factor. Only data with cloud fractions smaller than 0.2 according to the FRESCO cloud
676 data base (Wang et al., 2008) are used here. Furthermore, retrievals are limited to maximum
677 solar zenith angles of 85° for NO2 and 60° for HCHO. Uncertainties in NO_2 satellite
678 retrievals are large and depend on the region and season. Winter values in mid and high
679 latitudes are usually associated with larger error margins. As a rough estimate, systematic
680 uncertainties in regions with significant pollution are of the order of 20% – 30%. As the

HCHO retrieval is performed in the UV part of the spectrum where less light is available and the HCHO absorption signal is smaller than that of NO2, the uncertainty of monthly mean HCHO columns is relatively large (20% – 40%) and both noise and systematic offsets have an influence on the results. However, absolute values and seasonality are retrieved more accurately over HCHO hotspots.

For comparison to GOME-2 data, model data are vertically integrated without applying AK to tropospheric vertical columns of NO_2 and HCHO, interpolated to satellite observation time and then sampled to match the location of available cloud free satellite data, which has been gridded to match the model resolution. The resulting daily files are then averaged over months for both satellite and model data to reduce the noise.

3.3 Tropospheric Ozone

Figure 2 shows the monthly means of O_3 volume mixing ratios in the pressure ranges surface to 700 hPa (lower troposphere, LT) 700-400 hPa (middle troposphere, MT) and 400-200 hPa (upper troposphere UT) observed by sondes and averaged over Europe, North America and East Asia. Figure 3 shows the same as Figure 2 for the Tropics, Arctic and Antarctica. A more detailed breakdown of North America (Canada, Eastern and Western United States) and the Tropics (Atlantic/Africa, equatorial Americas and Eastern Indian Ocean/Western Pacific) following Times et al. (2012) is presented in the supplement. The observations have a pronounced spring maximum for UT O_3 over Europe, North America and East Asia and a more gradually developing maximum in late spring and summer in MT and LT. The LT seasonal cycle is well re-produced in all runs for the areas of the Northern Hemisphere (NH). In Europe, REAN tends to overestimate by about 5 ppb where the C-IFS and MOZ have almost no bias before the annual maximum in May apart from a small negative bias in spring. Later in the year, C-IFS tends to overestimate in autumn, whereas MOZ overestimates more in late summer. In MT over Europe C-IFS agrees slightly better with the observations than MOZ. MOZ overestimates in winter and spring and this overestimation is more prominent in the UT, where MOZ is biased high throughout the year. This overestimation in UT is highest in spring, where it can be 25% and more. These findings show that data assimilation in REAN improved UT O_3 considerably but had only little influence in LT and MT. The overestimation of MOZ in UT seems to be caused by increased stratospheric O_3 rather than a more efficient transport as lower stratospheric O_3 was overestimated in MOZ. Note that stratospheric ozone in C-IFS was nudged to the MACC re-analysis (see 3.1) but good agreement of C-IFS with

observation in UT in all three regions is also present in a run without nudging to stratospheric O_3. It is therefore not only a consequence of the use of assimilated observations in C-IFS (CB05).

Over North-America the spring time underestimation by C-IFS and MOZ is more pronounced than over Europe. The underestimation occurs in all regions but was largest in early spring over Canada. C-IFS also underestimates spring ozone throughout North America in MT. LT summer time ozone was overestimated in North America by all models, in particular over the Eastern United States. The bias of C-IFS was the smallest in LT but in contrast to MOZ and REAN C-IFS underestimates summer time ozone in MT over the Eastern United States. The overestimation of UT ozone by MOZ was most pronounced in Canada.

In East Asia all runs overestimate by 5-10 ppb in LT and MT especially in autumn and winter. In the northern high latitudes (Figure 3) the negative spring bias appears in all runs in LT and only for C-IFS in MT. As in the other regions, MOZ greatly overestimates UT O_3.

Averaged over the tropics, the annual variability is below 10 ppb with maxima in May and in September caused by the dry season in South-America (May) and Africa (September). The variability is well reproduced and biases are mostly below 5 ppb in the whole troposphere. Note that the 400-200 hPa range (UT) in the tropics is less influenced by the stratosphere because of the higher tropopause. C-IFS had smaller biases because of lower values in LT and higher values in MT and UT than MOZ. A more detailed analysis for different tropical regions shows that the seasonality is well captured by all models over Atlantic-Africa, equatorial America and eastern Indian Ocean/Western Pacific in all three tropospheric levels. However, the strong observed monthly anomalies (a observation glitch ? by one station) in equatorial America in March and September were underestimated by up to 20 ppb in all tropospheric levels.

Over the Arctic C-IFS and MOZ reproduce the seasonal cycle, which peaks in late spring, but generally underestimate the observations in LT. C-IFS had a smaller bias in LT than MOZ but had a larger negative bias in MT. The biggest improvement of C-IFS w.r.t to MOZ occurred at the surface in Antarctica as the biases compared to the GAW surface observations were greatly reduced. Notably, the assimilation (REAN) led to increased biases for LT and MT O_3, in particular during polar night when UV satellite observations are not available as already discussed in Flemming et al. (2011a).

744 The ability of the models to simulate O_3 near the surface is tested with rural AirBase and
745 EMEP stations (see section 3.2). Figure 4 shows monthly means and Figure 5 the average
746 diurnal cycle in different season in Europe. All runs underestimate monthly mean O_3 in spring
747 and winter and overestimate it in late summer and autumn. The overestimation in summer
748 was largest in MOZ. The recently reported (Val Martin at al. 2014) missing coupling of the
749 leaf area index to the leaf and stomatal vegetation resistance in the calculation of dry
750 deposition velocities could be an explanation of the MOZ bias. While the overestimation
751 appeared also with respect to the ozonesondes in LT (see Figure 2, left) the spring time
752 underestimation was less pronounced in LT.

753 The comparison of the diurnal cycle with observations (Figure 5) shows that C-IFS produced
754 a more realistic diurnal cycle than the MOZART model. The diurnal variability simulated by
755 the MOZART model is much less pronounced than the observations suggest. The diurnal
756 cycle of C-IFS and REAN were similar. This finding can be explained by the fact that C-IFS
757 and REAN use the IFS diffusion scheme whereas MOZART applies the diffusion scheme of
758 the MOZART CTM.

759 The negative bias of C-IFS in winter and spring seems mainly caused by an underestimation
760 of the night time values whereas the overestimation of the summer and autumn average values
761 in C-IFS were caused by an overestimation of the day time values. However, the
762 overestimation of the summer night time values by MOZART seems to be a strong
763 contribution to the average overestimation in this season.

764 ### 3.4 Carbon Monoxide

765 The seasonality of CO is mainly driven by its chemical lifetime, which is lower in summer
766 because of increased photochemical activity. The seasonal cycle of the CO emissions plays
767 also an important role in the case of biomass burning and high anthropogenic emissions. The
768 global distribution of total column CO retrieved from MOPITT and from AK weighted
769 columns simulated by C-IFS, MOZ and REAN is shown for April 2008 in Figure 6 and for
770 August in Figure 7. Figures showing the corresponding biases can be found in the
771 supplement. April and August have been selected because they are the months of the NH CO
772 maximum and minimum. C-IFS reproduced well the location of the observed global maxima
773 in North-America, Europe and China as well as the biomass burning signal in Central Africa.
774 However, there was a widespread underestimation of the MOPITT values in the NH, which
775 was strongest over European Russia and Northern China. Tropical CO was slightly

776 overestimated but more strongly over Southeast Asia in April at the end of the biomass
777 burning season in this region. The lower CO columns in mid- and high latitudes in the
778 Southern Hemisphere (SH) were underestimated. The same global gradients of the bias were
779 found in MOZ and REAN. The negative NH bias in April of MOZ is however more
780 pronounced but the positive bias in the tropics is slightly reduced. The bias of MOZ seems
781 stronger over the entire land surface in NH and not predominately in the areas with high
782 emission. This is consistent with the finding of Stein et al. (2014) that dry deposition, besides
783 underestimated emissions, contributes to the large negative biases in NH in MOZ.
784 Assimilating MOPITT (V4) in REAN led to much reduced biases everywhere even though
785 the sign of bias in NH, Tropics and SH remained. In August, the NH bias is reduced but the
786 hemispheric pattern of the CO bias was similar as in April for all runs. The only regional
787 exception from the general overestimation in the tropics is the strong underestimation of CO
788 in the biomass burning maximum in Southern Africa, which points to an underestimation of
789 the GFAS biomass burning emissions in that area.

790 More insight into the seasonal cycle and the vertical CO distribution can be obtained from
791 MOZAIC aircraft profiles. CO profiles at Frankfurt (Figure 8, left) provide a continuous
792 record with about 2 - 6 observations per day. As already reported in Inness et al. (2013) and
793 Stein et al. (2014), MOZ underestimates strongly LT CO with a negative bias of 40 - 60 ppb
794 throughout the whole year. The highest underestimation occurred in April and May, i.e. at the
795 time of the observed CO maximum. C-IFS CB05 also underestimates CO but with a smaller
796 negative bias in the range of 20-40 ppb even though it used the same CO emission data as
797 MOZ. REAN has the lowest bias throughout the year but the improvement is more important
798 in winter and early spring. The comparison over London, which is representative for 4 and 22
799 UTC, leads to similar results as for Frankfurt (Figure 8, middle). The seasonal variability of
800 LT CO from MOZAIC and the model runs in North-America is very similar to the one in
801 Europe (Figure 8, right). The late winter and spring bias is slightly increased whereas the
802 summer time bias was lower for all models. The surface bias in winter and spring of MOZ, C-
803 IFS and REAN is about -50, -40 and -20 ppb respectively. In the rest of the year REAN and
804 C-IFS have a bias of about -15 ppb whereas the bias of MOZ is about twice as large.

805 MT CO was very well produced by REAN in Europe and North-America probably because
806 MOPITT has the highest sensitivity at this level. The MT bias of C-IFS is about 75% of the
807 bias of MOZ, which underestimates by about 30 ppb. In the UT the CO biases are for all

808 models mostly below 10ppb, i.e. about 10 %. C-IFS has overall the smallest CO bias whereas
809 REAN tends to overestimate and MOZ to underestimate CO over Europe and North America.

810 CO observed by MOZAIC over Windhoek (Figure 9, middle) has a pronounced maximum in
811 September because of the seasonality of biomass burning in this region. Although all runs
812 show increased CO in this period, the models without assimilation were less able to reproduce
813 the high observed CO values and are biased low up to 40 ppb in LT and MT. Biases were
814 much reduced, i.e. mostly within 10 ppb, during the rest of the year. The assimilation in
815 REAN greatly reduces the bias in the biomass burning period. In UT C-IFS had slightly
816 smaller biases of about 10 ppb than MOZ and REAN. A less complete record of the seasonal
817 variability is available for Caracas (Figure 9, left). All models tend to underestimate UT and
818 MT CO maxima in April by about 20% but in contrast to Windhoek the C-IFS and not REAN
819 has the smallest bias in LT. Hyderabad (Figure 9, right) is the only observation site were a
820 substantial overestimation of CO in LT and UT is present even though the observations are in
821 the range of 150 - 250 ppb, which is mostly higher than at any of the other airports discussed.
822 All models overestimate the seasonality because of an underestimation in JJA and an
823 overestimation during the rest of the year.

824 The outcome of the comparison with LT CO from MOZAIC is consistent with the model bias
825 with respect to the GAW surface observations in Europe (Figure 10). The winter biases were
826 larger than summer biases and MOZ showed the largest understimation. ,. The GAW stations
827 measuring CO are mostly located on mountains in the Alpine region and typical annual biases
828 were about - 5, -20 and -35 ppb for REAN, C-IFS and MOZ respectively. The negative
829 biases of stations in flatter terrain such as Kollumerward tended to be larger.

830 ### 3.5 Nitrogen dioxide

831 The global maxima of NO_2 are located in areas of high anthropogenic and biomass burning
832 NO emissions. The global annual distribution of annual tropospheric columns retrieved from
833 the GOME-2 instrument and simulated by the models is shown in Figure 11. C-IFS, MOZ and
834 REAN showed a very similar distribution, which can be explained by that fact that the same
835 NO emission data were used in all runs. The global patterns of the modelled fields resemble
836 the observed annual patterns to a large extent. But the models tend to underestimate the high
837 observed values in East-Asia and Europe and also simulate too little NO_2 in larger areas of
838 medium observed NO_2 levels in Asia and Central Africa as well as in the outflow areas over
839 the West-Atlantic and West Pacific Ocean. This could mean that NO emissions in the most

polluted areas are too low but also that the simulated lifetime of NO_2 is too short. Further, an insufficient simulation of NO_x reservoir species such as PAN and the lack of alkyl nitrates in CB05 might be the reason for the underestimation.

The validation of the seasonality of NO_2 (Figure 12) for different regions and months shows that tropospheric NO_2 columns over Europe, North America, South Africa and East-Asia are reasonably reproduced. The models tend to underestimate tropospheric columns over Europe in summer (see Table 2 for area descriptions). However, the evaluation with GAW surface stations mainly from Central and Eastern Europe (Figure 13) revealed an overestimation by all models in winter and a small overestimation in summer for REAN and C-IFS. All runs significantly underestimate the annual cycle of the GOME-2 NO_2 tropospheric columns over East-Asia. The winter time values are only half of the observations whereas in summer models agree well with observations. In Southern Africa (20°S/0°S/15°E/15°W), the models overestimate the increased NO_2 values in the biomass burning season by a factor 2 but show good agreement with observations in the rest of the year. The overestimation during biomass burning events could be related to the assumed NO emission factor.

3.6 HCHO

On the global scale HCHO is mainly chemically produced by the oxidation of isoprene and CH_4. Isoprene is emitted by vegetation. On the regional scale HCHO emissions from anthropogenic sources, vegetation and biomass burning also contribute to the HCHO burden.

The annual average of tropospheric HCHO retrieved from GOME-2 and from the model runs is shown in Figure 14. The observations show higher values in the tropics and the NH and maxima in the rain forest regions of South America and Central Africa and in South East Asia. The simulated fields of the three runs are very similar. C-IFS, MOZ and REAN reproduce the observed global patterns but show a small but widespread underestimation in the NH extra-Tropics and in industrialized East Asia. On the other hand HCHO is overestimated in Indonesia. Figure 15 shows model time series of tropospheric HCHO against corresponding GOME-2 satellite retrievals for selected regions. The models underestimated satellite values over East-Asia especially in summer and overestimate HCHO columns for Indonesia (5°S/5°N/100°E/120°E) throughout the year. The seasonality in Southern Africa (not shown) and tropical South America (10°S/5°S/73°W/35°W) is well captured in particular by C-IFS. All models also reproduced the observations rather well for the Eastern United

States (30°N/40°N/90°W/75°W), but tend to underestimate wintertime HCHO columns for this region.

3.7 Sulfur dioxide

SO_2 was evaluated with available GAW surface observations from Central and Eastern Europe. There were considerable differences in the performance for individual stations often caused by local effects not resolved by the models. To summarize the evaluation for SO_2 Figure 16 shows the median of weekly observed and modelled time series. REAN and MOZ greatly exaggerated the seasonal cycle since the values in winter were up to eight times larger than the median of the observations. The summer values of the two runs were about 50% higher than the observations. C-IFS followed better the weak seasonality of the observations but suffered from a nearly constant bias of about 1 ppb (100%), which was much smaller than the bias of REAN and MOZ in winter but slightly higher in summer. Overall, the on-line integration of C-IFS showed lower SO_2 biases.

As no SO_2 observations were assimilated in REAN and identical SO_2 emission were used, the differences between the runs were caused by differences in the simulation of vertical mixing, sulphur chemistry and wet and dry deposition in C-IFS and MOZART. The winter time bias of REAN and MOZ could be introduced by the diffusion scheme in MOZART.

3.8 Computational cost

The computational cost is an important factor for the operational applications in CAMS. The computational cost of different configurations of IFS, C-IFS and IFS-MOZART are given in Table 3. Computational cost is expressed in billing units (BU) of the ECMWF IBM Power 7 super-computer. BUs are proportional to the number of used Central Processing Unit (CPU) times the simulation time.

The increase of cost because of the simulation of the CB05 chemistry with respect to an NWP run is about a factor 4 at the resolutions T159 (110km), T255 (80 km) and T511 (40 km). C-IFS (CB05) is about 8 times more efficient than the coupled system IFS-MOZART at a T159 resolution and about 15 times more at a T255 resolution. This strong relative increase in cost of IFS-MOZART is caused by the increasing memory requirements of the IFS at higher resolution, or also in data assimilation mode. However, there is insufficient parallelism in MOZART to exploit the larger number of CPU for speeding up the simulation of the coupled system.

C-IFS with the MOZART chemical mechanism, i.e. the same chemistry scheme as in IFS-MOZART, is about 2 times and C-IFS with RACMOBUS 7 times more costly than C-IFS (CB05) at a T159 resolution. Both the MOZART and the RACMOBUS schemes encompass a larger number of species and reactions and include a full stratospheric chemistry scheme, which is missing in CB05. The overhead because of the doubled number of advected species in C-IFS RACMOBUS and MOZART is however small because of the efficency of the SL advection scheme.

4 Summary and outlook

Modules for the simulation of atmospheric chemistry have been implemented on-line in the Integrated Forecasting System (IFS) of ECMWF. The chemistry scheme complements the already integrated modules for aerosol and greenhouse gases as part of the IFS for atmospheric composition (C-IFS). C-IFS for chemistry replaces the coupled system IFS-MOZART for forecast and assimilation of reactive gases within the pre-operational Copernicus Atmosphere Monitoring Service.

C-IFS applies the chemical mechanism CB05, which describes tropospheric chemistry with 55 species and 126 reactions. C-IFS benefits from the detailed cloud and precipitation physics of the IFS for the calculation of wet deposition and lightning NO emission. Wet deposition modelling is based on Jacob (2000) and accounts for the sub-grid scale distribution of clouds and precipitation. Dry deposition is modelled using pre-calculated monthly-mean dry deposition velocities following (Wesely, 1989) with a superimposed diurnal cycle. Surface emissions and dry depostion fluxes are applied as surface boundary condtions of the diffusion scheme. Lightning emissions of NO can be calculated either by cloud height (Price and Rind, 1993) or by convective precipitation (Meijer et al., 2001). The latter parameterization was used in this study. The anthropogenic emissions were taken from the MACCity inventory and biomass burning emissions from the GFAS data set for 2008.

An evaluation for the troposphere of a simulation in 2008 with C-IFS (CB05) and the MOZART CTM (MOZ) as well as with the MACC re-analysis (REAN) was carried out. The model results were compared against ozonesondes, MOZAIC CO aircraft profiles, European surface observations of O_3, CO, SO_2 and NO_2 and global satellite retrievals of CO, NO_2 and HCHO. The evaluation showed that C-IFS preforms better or with similar accuracy as MOZART and mostly of similar quality as the MACC re-analysis. It should be noted that

933 satellite retrievals of CO, O_3 and NO_2 were assimilated in the MACC re-analysis to improve
934 the realism of the fields simulated by IFS-MOZART.

935 In comparison to MOZ, C-IFS (CB05) had smaller biases (i) for CO in the Northern
936 Hemisphere, (ii) for O_3 in the upper troposphere and (ii) for winter-time SO_2 at the surface in
937 Europe. Further, the diurnal cycle of surface O_3, tested with rural European Air quality
938 observations, showed greater realism in the C-IFS simulation. As both models used the same
939 emission data, the improvements can be explained by the differences in the chemical
940 mechanism and the simulation of wet and dry deposition. However, the improvements in SO_2
941 and the diurnal cycle of O_3 are most probably caused by the more consistent interplay of
942 diffusion and sink and sources processes in the on-line integrated C-IFS.

943 There is still room for improvement of C-IFS (CB05). It underestimated surface O_3 over
944 Europe and North America in spring and overestimated it in late summer and autumn. CO
945 was still underestimated by C-IFS in particular in Europe and North America throughout the
946 year but more in spring and winter, and in the biomass burning season in Africa. Winter time
947 tropospheric NO_2 over China as retrieved from the GOME-2 instrument was two times higher
948 than the fields modelled by C-IFS, MOZART and the MACC re-analysis.

949 Although only one chemical mechanism is described in the paper, C-IFS is a model that can
950 apply multiple chemistry schemes. The implementation of the chemistry schemes of the
951 CTMs MOCAGE and MOZART has technically been completed but further optimisation and
952 evaluation is required. Both schemes offer a description of stratospheric chemistry, which is
953 not included in the tropospheric scheme CB05. For this reason it is intended to combine the
954 CB05 mechanism with the BASCOE stratospheric mechanism. An inter-comparison of the
955 performance of the different chemical mechanism is planned.

956 It is foreseen to further improve the link between the physics and chemistry packages in IFS.
957 For example, the detailed information from the IFS surface scheme will be utilised for the
958 calculation of dry deposition and biogenic emissions. A first important step is to replace the
959 climatological dry deposition velocities with-online calculated values. Further, the impact of
960 the simulated O_3 fields, once the stratospheric chemistry is fully implemented, on the IFS
961 radiation scheme and the corresponding feedback on the temperature fields will be
962 investigated.

963 Another ongoing development is to link more closely the greenhouse gas, aerosol and gas-
964 phase chemistry modules of C-IFS. Relevant chemical conversion terms can already be fed to

965 the GLOMAP aerosol (Mann et al, 2010) module for the simulation of secondary aerosols.
966 The calculation of photolysis rates can account for the presence of aerosols, and HO_2 uptake
967 on aerosols can be simulated (Huijnen et al., 2014).

968 In summary, C-IFS is a new global chemistry weather model for forecast and assimilation of
969 atmospheric composition. C-IFS (CB05) has already been successfully applied in data
970 assimilation mode (Inness et al., 2015). C-IFS offers improvements over the coupled system
971 IFS-MOZART because (i) it simulates several trace gas C-IFS (CB05)es with better accuracy,
972 (ii) it is computational several times more efficient in particular at high resolution and (iii) it
973 better facilitates the implementation of feedback processes between gas-phase and aerosol
974 processes as well as between atmospheric composition and meteorology.

975 **Acknowledgments**

976 MACC II is funded by the European Union's Seventh Framework Programme (FP7) under
977 Grant Agreement no. 283576. The MOPITT data were obtained from the NASA Langley
978 Research Atmospheric Science Data Center. We are grateful to the World Ozone and
979 Ultraviolet Radiation Data Centre (WOUDC) for providing ozonesonde obervations. We
980 thank the Global Atmospheric Watch programme for the provision of NO_2, CO and SO_2
981 surface observations. We thank the European Environmental Agency for providing access to
982 European O_3 observations in the AirBase data base. We also thank the MOZAIC
983 (Measurements of OZone, water vapour, carbon monoxide and nitrogen oxides by in-service
984 AIrbus aircraft) and IAGOS (In-Service Aircraft for a Global Observing System) programmes
985 for providing CO profile observations.

986

987 **Code Availability**

988 The C-IFS source code is integrated in ECWMF's IFS code, which is only available subject to
989 a licence agreement with ECMWF. ECMWF member-state weather services and their
990 approved partners will get access granted. The IFS code without modules for assimilation and
991 chemistry can be obtained for educational and academic purposes as part of the openIFS
992 release (https://software.ecmwf.int/wiki/display/OIFS/OpenIFS+Home). A detailed
993 documentation of the IFS code is available from
994 https://software.ecmwf.int/wiki/display/IFS/CY40R1+Official+IFS+Documentation. The
995 CB05 chemistry module of C-IFS was originally developed in the TM5 chemistry-transport

model. Readers interested in the TM5 code can contact the TM5 developers (http://tm5.sourceforge.net) or can go directly to the TM5 wiki page, http://tm.knmi.nl/index.php/Main_Page.

References

Archibald, A. T., Cooke, M. C., Utembe, S. R., Shallcross, D. E., Derwent, R. G., and Jenkin, M. E.: Impacts of mechanistic changes on HOx formation and recycling in the oxidation of isoprene, Atmos. Chem. Phys., 10, 8097-8118, doi:10.5194/acp-10-8097-2010, 2010.

Arnold, S. R., Emmons, L. K., Monks, S. A., Law, K. S., Ridley, D. A., Turquety, S., Tilmes, S., Thomas, J. L., Bouarar, I., Flemming, J., Huijnen, V., Mao, J., Duncan, B. N., Steenrod, S., Yoshida, Y., Langner, J., and Long, Y.: Biomass burning influence on high latitude tropospheric ozone and reactive nitrogen in summer 2008: a multi-model analysis based on POLMIP simulations, Atmos. Chem. Phys. Discuss., 14, 24573-24621, doi:10.5194/acpd-14-24573-2014, 2014.

Atkinson, R., Baulch, D. L., Cox, R. A., Crowley, J, N., Hampson, R. F., Hynes, R. G., Jenkin, M. E., Rossi, M. J. and Troe, J.: Evaluated kinetic and photochemical data for atmospheric chemistry: Volume I – gas phase reactions of Ox, HOx, NOx and SOx, species, Atmos. Chem. Phys., 4, 1461–1738, doi:10.5194/acp-4-1461-2004, 2004.

Atkinson, R., Baulch, D. L., Cox, R. A., Crowley, J. N., Hampson, R. F., Hynes, R. G., Jenkin, M. E., Rossi, M. J., Troe, J., and IUPAC Subcommittee: Evaluated kinetic and photochemical data for atmospheric chemistry: Volume II – gas phase reactions of organic species, Atmos. Chem. Phys., 6, 3625–4055, doi:10.5194/acp-6-3625-2006, 2006.

Baklanov, A., Schlünzen, K., Suppan, P., Baldasano, J., Brunner, D., Aksoyoglu, S., Carmichael, G., Douros, J., Flemming, J., Forkel, R., Galmarini, S., Gauss, M., Grell, G., Hirtl, M., Joffre, S., Jorba, O., Kaas, E., Kaasik, M., Kallos, G., Kong, X., Korsholm, U., Kurganskiy, A., Kushta, J., Lohmann, U., Mahura, A., Manders-Groot, A., Maurizi, A., Moussiopoulos, N., Rao, S. T., Savage, N., Seigneur, C., Sokhi, R. S., Solazzo, E., Solomos, S., Sørensen, B., Tsegas, G., Vignati, E., Vogel, B., and Zhang, Y.: Online coupled regional meteorology chemistry models in Europe: current status and prospects, Atmos. Chem. Phys., 14, 317-398, doi:10.5194/acp-14-317-2014, 2014.

Banda, N., Krol, M, van Noije, T. , van Weele, M. , Williams, J. E., Le Sager, P. , Niemeier, U., Thomason, L. and Röckmann, T. : The effect of stratospheric sulfur from Mount Pinatubo on tropospheric oxidizing capacity and methane, J. Geophys. Res. Atmos., 119, doi:10.1002/2014JD022137, 2014.

1031

1032 Barkley, M., Description of MEGAN biogenic VOC emissions in GEOS-Chem, 2010.
1033 http://acmg.seas.harvard.edu/geos/wiki_docs/emissions/megan.pdf

1034 Bechtold, P., Semane, N., Lopez, P., Chaboureau, J-P, Beljaars, A., Bormann, N: 2014:
1035 Representing Equilibrium and Nonequilibrium Convection in Large-Scale Models. J. Atmos.
1036 Sci., 71, 734–753. doi: http://dx.doi.org/10.1175/JAS-D-13-0163.1. 2014.

1037 Beekmann M., Ancellet G., Megie G., Smit H. G. J., and Kley D.: Intercomparison campaign
1038 for vertical ozone profiles including electrochemical sondes of ECC and Brewer-Mast type
1039 and aground based UV-differential absorption radar, J. Atmos. Chem., 10, 259–288, 1994.

1040 Beljaars, A. and Viterbo, P.: The role of the boundary layer in a numerical weather prediction
1041 model, in: Clear and cloudy boundary layers, A.A.M. Holtslag and P. Duynkerke (eds.),
1042 Royal Netherlands Academy of Arts and Sciences, p. 287-304, Amsterdam, North Holland
1043 Publishers, 1998.

1044 Beljaars, A., Bechtold, P., Kohler, M., Morcrette, J-J., Tompkins, A., Viterbo, P. and Wedi,
1045 N.: The numerics of physical parameterization, Seminar on Recent developments in
1046 numerical methods for atmospheric and ocean modelling, 6-10 September,
1047 http://www.ecmwf.int/publications/library/do/references/, 2004.

1048 Benedetti, A., Morcrette, J.-J., Boucher, O., Dethof, A., Engelen, R. J., Fisher, M., Flentje, H.,
1049 Huneeus, N., Jones, L.,Kaiser, J. W., Kinne, S., Mangold, A., Razinger, M.,Simmons, A. J.,
1050 Suttie, M., and the GEMS-AER team: Aerosol analysis and forecast in the European Centre
1051 for Medium-Range Weather Forecasts Integrated Forecast System: 2. Data assimilation, J.
1052 Geophys. Res., 114, D13205, doi:10.1029/2008JD011115, 2009.

1053 Bousserez, N., Attié, J.-L., Peuch, V.-H., Michou, M., and Pfister, G.: Evaluation of the
1054 MOCAGE chemistry and transport model during the ICARTT/ITOP experiment, J. Geophys.
1055 Res., 112, D10S42, doi:10.1029/2006JD007595, 2007.

1056 Callies, J., Corpacicioli, E., Eisinger, M., Hahne, A., and Lefebvre, A.: GOME-2 Metops's
1057 Second Generation Sensor for Operational Ozone Monitoring, ESA Bulletin, 102, 2000.

1058 Cariolle, D. and Deque, M.:. Southern hemisphere medium-scale waves and total ozone
1059 disturbances in a spectral general circulation model, J. Geophys. Res., 91D, 10825–10846,
1060 1986.

1061 Cariolle, D. and Teyssèdre, H.: A revised linear ozone photochemistry parameterization for
1062 use in transport and general circulation models: multi-annual simulations, Atmos. Chem.
1063 Phys., 7, 2183-2196, doi:10.5194/acp-7-2183-2007, 2007.

1064 Carslaw, K. S., Luo, B., Peter, T., and Clegg, S. L.: Vapour pressures of
1065 H2SO4/HNO3/HBr/H2O solutions to low stratospheric temperatures, Geophys. Res. Lett., 22,
1066 247-250, 1995.

1067 Cecil, D.J., Buechler, D. E., Blakeslee, R. J. : Gridded lightning climatology from TRMM-
1068 LIS and OTD: Dataset description, Atmospheric Research, 135–136, 404-414,
1069 doi:10.1016/j.atmosres.2012.06.028, 2012.

1070 Chin, M., D. J. Jacob, G. M. Gardner, M. S. Foreman-Fowler, P. A. Spiro, and D. L. Savoie:
1071 A global three-dimensional model of tropospheric sulfate, J. Geophys. Res., 101, (D13),
1072 18,667–18,690, 1996

1073 DeCaria, A. J., Pickering, K. E. , Stenchikov, G. L. and Ott, L. E.: Lightning-generated NO_X
1074 and its impact on tropospheric ozone production: A three-dimensional modeling study of a
1075 Stratosphere-Troposphere Experiment: Radiation, Aerosols and Ozone (STERAO-A)
1076 thunderstorm, J. Geophys. Res., 110, D14303, doi:10.1029/2004JD005556, 2005.

1077 Dee, D.P., Uppala, S.M., Simmons, A.J., Berrisford, P., Poli, P., Kobayashi, S., Andrae, U.,
1078 Balmaseda, M.A., Balsamo, G., Bauer, P., Bechtold, P., Beljaars, A.C.M., van de Berg, L.,
1079 Bidlot, J., Bormann, N., Delsol, C., Dragani, R., Fuentes, M., Geer, A.J., Haimberger, L.,
1080 Healy, S.B., Hersbach, H., Hólm, E.V., Isaksen, L., Kållberg, P., Köhler, M., Matricardi, M.,
1081 Mcnally, A.P., Monge-Sanz, B.M., Morcrette, J.-J., Park, B.-K., Peubey, C., de Rosnay, P.,
1082 Tavolato, C., Thépaut, J.-N., Vitart, F.: The ERA-Interim reanalysis: Configuration and
1083 performance of the data assimilation system, Quarterly Journal of the Royal Meteorological
1084 Society, 2011.

1085 Deeter, M. N., S. Martínez-Alonso, D. P. Edwards, L. K. Emmons, J. C. Gille, H. M. Worden,
1086 J. V. Pittman, B. C. Daube, and S. C. Wofsy: Validation of MOPITT Version 5 thermal-
1087 infrared, near-infrared, and multispectral carbon monoxide profile retrievals for 2000–2011, J.
1088 Geophys. Res. Atmos., 118, 6710–6725, doi:10.1002/jgrd.50272, 2013a.

1089 Deeter, M.N., MOPITT Version 6 Product User's Guide, Technical Report, NCAR, Boulder,
1090 USA, 2013.137 (656), pp. 553-597, 2013b.

1091 Dentener, F. J. and Crutzen, P. J.: Reaction of N2O5 on tropospheric aerosols: Impact on the
1092 global distributions of NOx, O3 and OH, J. Geophys. Res., 98(D4), 7149–7163, 1993.

1093 Diamantakis, M. and Flemming, J.: Global mass fixer algorithms for conservative tracer
1094 transport in the ECMWF model, Geosci. Model Dev., 7, 965-979, doi:10.5194/gmd-7-965-
1095 2014, 2014.

1096 Elguindi, N., Clark, H., Ordóñez, C., Thouret, V., Flemming, J., Stein, O., Huijnen, V.,
1097 Moinat, P., Inness, A., Peuch, V.-H., Stohl, A., Turquety, S., Athier, G., Cammas, J.-P., and
1098 Schultz, M.: Current status of the ability of the GEMS/MACC models to reproduce the
1099 tropospheric CO vertical distribution as measured by MOZAIC, Geosci. Model Dev., 3, 501-
1100 518, doi:10.5194/gmd-3-501-2010, 2010.

1101 Emmons, L. K., Walters, S., Hess, P. G., Lamarque, J.-F., Pfister, G. G., Fillmore, D.,
1102 Granier, C., Guenther, A., Kinnison, D., Laepple, T., Orlando, J., Tie, X., Tyndall, G.,
1103 Wiedinmyer, C., Baughcum, S. L., and Kloster, S.: Description and evaluation of the Model
1104 for Ozone and Related chemical Tracers, version 4 (MOZART-4), Geosci. Model Dev., 3, 43-
1105 67, doi:10.5194/gmd-3-43-2010, 2010.

1106 Emmons, L.K., Arnold, S., Monks, S., Huijnen, V., Tilmes, S., Law, K., Thomas, J.L., Raut,
1107 J-C., Bouarar, I., Turquety, S., Long, Y., Duncan, B., Steenrod, S., Strode, S., Flemming, J.
1108 Mao, J., Langner, J., Thompson, A., Tarasick, D., Apel, E., Blake, D., Brune, W., Cohen, R.,
1109 Dibb, J., Diskin, G. S., Fried, A., Hall, S., Huey, G., Weinheimer, ennberg, P., Wisthaler, A.,
1110 de Gouw, J., Holloway, J., Montzka, S., Nowak, J., Roberts, J. and Ryerson, J.: The
1111 POLARCAT Model Intercomparison Project (POLMIP): Overview and evaluation with
1112 observations, Atmospheric Chemistry and Physics, to be submitted, 2014.

1113 Engelen, R. J., Serrar, S., and Chevallier, F.: Four-dimensional data assimilation of
1114 atmospheric CO2 using AIRS observations, J. Geophys. Res., 114, D03303,
1115 doi:10.1029/2008JD010739, 2009.

1116 Errera, Q., Daerden, F., Chabrillat, S., Lambert, J. C., Lahoz, W. A., Viscardy, S., Bonjean,
1117 S., and Fonteyn, D.: 4D-Var assimilation of MIPAS chemical observations: ozone and
1118 nitrogen dioxide analyses, Atmos. Chem. Phys., 8, 6169-6187, doi:10.5194/acp-8-6169-2008,
1119 2008.

1120 Evans, M. J., and Jacob, D. J.: Impact of new laboratory studies of N2O5 hydrolysis on global
1121 model budgets of tropospheric nitrogen oxides, ozone, and OH, Geophys. Res. Lett., 32,
1122 L09813, doi:10.1029/2005GL022469, 2005.

Fiore, A.M., Naik, V., Spracklen, D.V., Steiner, A., Unger, N., Prather, M., Bergmann, D., Cameron-Smith, P.J., Cionni, I., Collins, W.J., Dalsoren, S., Eyring, V., Folberth, G.A., Ginoux, P., Horowitz, L.W., Josse, B., Lamarque, J.-F., MacKenzie, I.A., Nagashima, T., O'Connor, F.M., Righi, M., Rumbold, S.T., Shindell, D.T., Skeie, R.B., Sudo, K., Szopa, S., Takemura, T., Zeng, G., Global air quality and climate, Chemical Society Reviews, 41 (19), pp. 6663-6683, 2012.

Flemming, J., Stern, R., and Yamartino, R. J.: A new air quality regime classification scheme for O_3, NO_2, SO_2 and PM10 observations sites, Atmos. Environ., 39, 6121–6129, 2005

Flemming, J., Inness, A., Flentje, H., Huijnen, V., Moinat, P., Schultz, M. G., and Stein, O.: Coupling global chemistry transport models to ECMWF's integrated forecast system, Geosci. Model Dev., 2, 253-265, doi:10.5194/gmd-2-253-2009, 2009a.

Flemming, J., Inness, A., Flentje, H., Huijnen, V., Moinat, P., Schultz, M. G., and Stein, O.: Coupling global chemistry transport models to ECMWF's integrated forecast system ECMWF technical memorandum 590 [http://old.ecmwf.int/publications/library/ecpublications/_pdf/tm/501-600/tm590.pdf] tm590.pdf, 2009 b.

Flemming, J., Inness, A., Jones, L., Eskes, H. J., Huijnen, V., Schultz, M. G., Stein, O., Cariolle, D., Kinnison, D., and Brasseur, G.: Forecasts and assimilation experiments of the Antarctic ozone hole 2008, Atmos. Chem. Phys., 11, 1961–1977, doi:10.5194/acp-11-1961-2011, 2011 a.

Flemming, J. and Huijnen, V.: IFS Tracer Transport Study, MACC Deliverable G-RG 4.2, Tech. rep., ECMWF, http://www.gmes-atmosphere.eu/documents/deliverables/g-rg/ifs transport study.pdf, 2011 b.

Flemming, J.; Peuch, V.-H.; Engelen, R.; Kaiser, J.W. A European Global-to-Regional Air Pollution Forecasting System that Combines Modeling with Satellite Observations; EM Magazine of A&WMA, November 2013, pp. 6-10. https://www.researchgate.net/publication/259535688_A_European_Global-to-Regional_Air_Pollution_Forecasting_System_that_Combines_Modeling_with_Satellite_Observations, 2013

Forbes, R.M., A.M. Tompkins & A. Untch, A new prognostic bulk-microphysics scheme for the IFS. ECMWF Tech. Memo. No. 649, 2011.

1154 Fu, Q., Yang, P. and Sun, W. B.:. An accurate parametrization of the infrared radiative
1155 properties of cyrrus clouds of climate models. J. Climate, 11, 2223–2237, 1998

1156 Gauss, M., Isaksen, I. S. A., Lee, D. S., and Søvde, O. A.: Impact of aircraft NOx emissions
1157 on the atmosphere – tradeoffs to reduce the impact, Atmos. Chem. Phys., 6, 1529-1548,
1158 doi:10.5194/acp-6-1529-2006, 2006.

1159 Gery, M., Whitten, G. Z., Killus, J. P., and Dodge, M. C.: A photochemical kinetics
1160 mechanism for urban and regional scale computer modelling, J. Geophys. Res., 94, 18925–
1161 18956, 1989.

1162 Granier, C., J.F. Lamarque, A. Mieville, J.F. Muller, J. Olivier, J. Orlando, J. Peters, G.
1163 Petron, G. Tyndall, S. Wallens, POET, a database of surface emissions of ozone precursors,
1164 available on internet at http://www.aero.jussieu.fr/projet/ACCENT/POET.php , 2005.

1165 Granier, C., B. Bessagnet, T. Bond, A. D'Angiola, H.D.v.d. Gon, G.J. Frost, A. Heil, J.W.
1166 Kaiser, S. Kinne, Z. Klimont, S. Kloster, J.-F. Lamarque, C. Liousse, T. Masui, F. Meleux, A.
1167 Mieville, T. Ohara, J.-C. Raut, K. Riahi, M.G. Schultz, S.J. Smith, A. Thomson, J.v.
1168 Aardenne, G.R.v.d. Werf, and D.P.v. Vuuren, Evolution of anthropogenic and biomass
1169 burning emissions of air pollutants at global and regional scales during the 1980-2010 period,
1170 Climatic Change, 109(1-2), 163-190, doi:10.1007/s10584-011-0154-1, 2011.

1171 Grell, G. A., Peckham, S. E. , Schmitz, R , McKeen, S. A.,. Frost, G. J, Skamarock, W. and
1172 Eder B.: Fully coupled online chemistry within the WRF model, Atmospheric Environment ,
1173 39, 37, 6957-6975, 2005.

1174 Grooß, J.-U. and Russell III, J. M.: Technical note: A stratospheric climatology for O3, H2O,
1175 CH4, NOx, HCl and HF derived from HALOE measurements, Atmos. Chem. Phys., 5, 2797–
1176 2807, doi:10.5194/acp-5-2797-2005, 2005

1177 Guenther, A. B., Karl, T., Harley, P., Wiedinmyer, C., Palmer, P. I., and Geron, C.: Estimates
1178 of global terrestrial isoprene emissions using MEGAN (Model of Emissions of Gases and
1179 Aerosols from Nature), Atmos. Chem. Phys., 6, 3181–3210, doi:10.5194/acp-6-3181-2006,
1180 2006.

1181 Haywood, J. M., Roberts, D. L., Slingo, A., Edwards, J. M., and Shine, K. P.: General
1182 circulation model calculations of the direct radiative forcing by anthropogenic sulfate and
1183 fossil-fuel soot aerosol, Journal of Climate, 10, 1562–1577, 1997.

1184 Hertel, O., Berkowicz, R., Christensen, J. and Hov Ø: Test of two numerical schemes for use
1185 in atmospheric transport-chemistry models Atmos. Environ., 27A(16), 2591–2611, 1993.

1186 Hollingsworth, A., Engelen, R.J., Textor, C., Benedetti, A., Boucher, O. , Chevallier, F.,
1187 Dethof, A., Elbern, H., Eskes, H., Flemming, J., Granier, C., Kaiser, J.W. , Morcrette, J.-J.,
1188 Rayner, P., Peuch, V.H., Rouil, L., Schultz, M.G.,. Simmons, A.J and The GEMS
1189 Consortium: Toward a Monitoring and Forecasting System For Atmospheric Composition:
1190 The GEMS Project. Bull. Amer. Meteor. Soc., 89, 1147-1164, 2008.

1191 Holtslag, A.A. and B. Boville: Local versus nonlocal boundary-layer diffusion in a global
1192 climate model, J. Clim., 6, 1825-1842, 1993.

1193 Horowitz, L. W., Walters, S., Mauzerall, D. L., Emmons, L. K., Rasch, P. J., Granier, C., Tie,
1194 X., Lamarque, J.-F., Schultz, M. G., Tyndall, G. S., Orlando, J. J., and Brasseur, G. P.: A
1195 global simulation of tropospheric ozone and related tracers, Description and Evaluation of
1196 MOZART version 2, J. Geophys. Res., 108, 4784, doi:10.1029/2002JD002853, 2003.

1197 Hortal, M. and Simmons, A. J.: Use of reduced Gaussian grids in spectral models, Mon.
1198 Weather Rev., 119, 1057 1074, 1991.

1199 Hortal, M.: The development and testing of a new two-time-level semi-Lagrangian scheme
1200 (SETTLS) in the ECMWF forecast model, 128, 1671–1687, DOI: 10.1002/qj.200212858314,
1201 2002.

1202 Houweling, S., Dentener, F. J., and Lelieveld, J.: The impact of nonmethane hydrocarbon
1203 compounds on tropospheric photochemistry, J. Geophys. Res., 103(D9), 10673–10696, 1998.

1204 Huijnen, V., Williams, J., van Weele, M., van Noije, T., Krol, M., Dentener, F., Segers, A.,
1205 Houweling, S., Peters, W., de Laat, J., Boersma, F., Bergamaschi, P., van Velthoven, P., Le
1206 Sager, P., Eskes, H., Alkemade, F., Scheele, R., Nédélec, P., and Pätz, H.-W.: The global
1207 chemistry transport model TM5: description and evaluation of the tropospheric chemistry
1208 version 3.0, Geosci. Model Dev., 3, 445-473, doi:10.5194/gmd-3-445-2010.

1209 Huijnen, V., Flemming, J., Kaiser, J. W., Inness, A., Leitão, J., Heil, A., Eskes, H. J., Schultz,
1210 M. G., Benedetti, A., Hadji-Lazaro, J., Dufour, G., and Eremenko, M.: Hindcast experiments
1211 of tropospheric composition during the summer 2010 fires over western Russia, Atmos.
1212 Chem. Phys., 12, 4341-4364, doi:10.5194/acp-12-4341-2012, 2012.

1213 Huijnen, V., Williams, J. E., and Flemming, J.: Modeling global impacts of heterogeneous
1214 loss of HO2 on cloud droplets, ice particles and aerosols, Atmos. Chem. Phys. Discuss., 14,
1215 8575-8632, doi:10.5194/acpd-14-8575-2014, 2014.

1216 Im, U., Bianconi, R., Solazzo, E., Kioutsioukis, I., Badia, A., Balzarini, A., Baró, R., Bellasio,
1217 R., Brunner, D., Chemel, C., Curci, G., Flemming, J., Forkel, R., Giordano, L., Jiménez-
1218 Guerrero, P., Hirtl, M., Hodzic, A., Honzak, L., Jorba, O., Knote, C., Kuenen, J.J.P., Makar,
1219 P.A., Manders-Groot, A., Neal, L., Pérez, J.L., Pirovano, G., Pouliot, G., San Jose, R.,
1220 Savage, N., Schroder, W., Sokhi, R.S., Syrakov, D., Torian, A., Tuccella, P., Werhahn, J.,
1221 Wolke, R., Yahya, K., Zabkar, R., Zhang, Y., Zhang, J., Hogrefe, C., Galmarini, S.:
1222 Evaluation of operational on-line-coupled regional air quality models over Europe and North
1223 America in the context of AQMEII phase 2. Part I: Ozone, Atmospheric Environment , doi:
1224 10.1016/j.atmosenv.2014.09.042, 2014.

1225 Inness, A., Baier, F., Benedetti, A., Bouarar, I., Chabrillat, S., Clark, H., Clerbaux, C.,
1226 Coheur, P., Engelen, R. J., Errera, Q., Flemming, J., George, M., Granier, C., Hadji-Lazaro,
1227 J., Huijnen, V., Hurtmans, D., Jones, L., Kaiser, J. W., Kapsomenakis, J., Lefever, K., Leitão,
1228 J., Razinger, M., Richter, A., Schultz, M. G., Simmons, A. J., Suttie, M., Stein, O., Thépaut,
1229 J.-N., Thouret, V., Vrekoussis, M., Zerefos, C., and the MACC team: The MACC reanalysis:
1230 an 8 yr data set of atmospheric composition, Atmos. Chem. Phys., 13, 4073-4109,
1231 doi:10.5194/acp-13-4073-2013, 2013.

1232

1233 Inness, A., Blechschmidt, A.-M., Bouarar, I., Chabrillat, S., Crepulja, M., Engelen, R. J.,
1234 Eskes, H., Flemming, J., Gaudel, A., Hendrick, F., Huijnen, V., Jones, L., Kapsomenakis, J.,
1235 Katragkou, E., Keppens, A., Langerock, B., de Mazière, M., Melas, D., Parrington, M.,
1236 Peuch, V. H., Razinger, M., Richter, A., Schultz, M. G., Suttie, M., Thouret, V., Vrekoussis,
1237 M., Wagner, A., and Zerefos, C.: Data assimilation of satellite retrieved ozone, carbon
1238 monoxide and nitrogen dioxide with ECMWF's Composition-IFS, Atmos. Chem. Phys.
1239 Discuss., 15, 4265-4331, doi:10.5194/acpd-15-4265-2015, 2015.

1240 Jacob, D.J. H. Liu, C.Mari, and R.M. Yantosca, Harvard wet deposition scheme for GMI,
1241 Harvard University Atmospheric Chemistry Modeling Group, revised March 2000.
1242 http://acmg.seas.harvard.edu/geos/wiki_docs/deposition/wetdep.jacob_etal_2000.pdf

1243 Jakob, C. and Klein, S.: A parameterization of the effects of cloud and precipitation overlap
1244 for use in general-circulation models, Q. J. Roy. Meteor. Soc., 126, 2525–2544, 2000.

1245 Jung, T., T. N. Palmer, M. J. Rodwell, and S. Serrar, 2008: Diagnosing forecast error using
1246 relaxation experiments. ECMWF Newsletter 82, ECMWF, Shinfield Park, Reading, Berkshire
1247 RG2 9AX, UK.

1248 Kaiser, J. W., Heil, A., Andreae, M. O., Benedetti, A., Chubarova, N., Jones, L., Morcrette,
1249 J.-J., Razinger, M., Schultz, M. G., Suttie, M., and van der Werf, G. R.: Biomass burning
1250 emissions estimated with a global fire assimilation system based on observed fire radiative
1251 power, Biogeosciences, 9, 527-554, doi:10.5194/bg-9-527-2012, 2012.

1252 Kaminski, J. W., Neary, L., Struzewska, J., McConnell, J. C., Lupu, A., Jarosz, J., Toyota, K.,
1253 Gong, S. L., Côté, J., Liu, X., Chance, K., and Richter, A.: GEM-AQ, an on-line global
1254 multiscale chemical weather modelling system: model description and evaluation of gas phase
1255 chemistry processes, Atmos. Chem. Phys., 8, 3255-3281, 2008.

1256 Kinnison, D. E., Brasseur, G. P., Walters, S. , Garcia, R. R.,. Marsh, D. R , Sassi, F., Harvey,
1257 V. L., Randall, C. E., Emmons, L., Lamarque, J. F., Hess, P. , Orlando, J. J., Tie, X. X. ,
1258 Randel, W. , Pan, L. L., Gettelman, A. , Granier, C., Diehl, T., Niemeier, U. and Simmons, A.
1259 J.: Sensitivity of Chemical Tracers to Meteorological Parameters in the MOZART-3
1260 Chemical Transport Model. J. Geophys. Res, 112, D03303, doi:10.1029/2008JD010739,2007.

1261 Komhyr, W. D., Barnes, R. A., Borthers, G. B., Lathrop, J. A., Kerr, J. B., and Opperman, D.
1262 P.: Electrochemical concentration cell ozonesonde performance evaluation during STOIC
1263 1989, J. Geophys. Res., 100, 9231–9244, 1995

1264 Lamarque, J.-F., Emmons, L. K., Hess, P. G., Kinnison, D. E., Tilmes, S., Vitt, F., Heald, C.
1265 L., Holland, E. A., Lauritzen, P. H., Neu, J., Orlando, J. J., Rasch, P. J., and Tyndall, G. K.:
1266 CAM-chem: description and evaluation of interactive atmospheric chemistry in the
1267 Community Earth System Model, Geosci. Model Dev., 5, 369-411, doi:10.5194/gmd-5-369-
1268 2012, 2012.

1269 Lamarque, J.-F., Shindell, D. T., Josse, B., Young, P. J., Cionni, I., Eyring, V., Bergmann, D.,
1270 Cameron-Smith, P., Collins, W. J., Doherty, R., Dalsoren, S., Faluvegi, G., Folberth, G.,
1271 Ghan, S. J., Horowitz, L. W., Lee, Y. H., MacKenzie, I. A., Nagashima, T., Naik, V.,
1272 Plummer, D., Righi, M., Rumbold, S. T., Schulz, M., Skeie, R. B., Stevenson, D. S., Strode,
1273 S., Sudo, K., Szopa, S., Voulgarakis, A., and Zeng, G.: The Atmospheric Chemistry and
1274 Climate Model Intercomparison Project (ACCMIP): overview and description of models,

1275 simulations and climate diagnostics, Geosci. Model Dev., 6, 179-206, doi:10.5194/gmd-6-
1276 179-2013, 2013.

1277 Landgraf, J. and Crutzen, P. J.: An efficient method for online calculations of photolysis and
1278 heating trates, J. Atmos. Sci., 55, 863–878, 1998.

1279 Lawrence, M.G. and Crutzen, P. J: The impact of cloud particle gravitational settling on
1280 soluble trace gas distributions. Tellus B, 50: 263–289. doi: 10.1034/j.1600-0889.1998.

1281 Lefever, K., van der A, R., Baier, F., Christophe, Y., Errera, Q., Eskes, H., Flemming, J.,
1282 Inness, A., Jones, L., Lambert, J.-C., Langerock, B., Schultz, M. G., Stein, O., Wagner, A.,
1283 and Chabrillat, S.: Copernicus atmospheric service for stratospheric ozone: validation and
1284 intercomparison of four near real-time analyses, 2009–2012, Atmos. Chem. Phys. Discuss.,
1285 14, 12461-12523, doi:10.5194/acpd-14-12461-2014, 2014.

1286 Levine, S. Z. and Schwartz, S. E.: In-cloud and below-cloud scavenging of nitric acid vapor.
1287 Atmos. Environ. doi:10.1016/0004-6981(82)90266-9, 1982.

1288 Lin, J.-T., McElroy, M. B., and Boersma, K. F.: Constraint of anthropogenic NOx emissions
1289 in China from different sectors: a new methodology using multiple satellite retrievals, Atmos.
1290 Chem. Phys., 10, 63-78, doi:10.5194/acp-10-63-2010, 2010.

1291 Liu, H., Jacob, D.J., Bey, I., Yantosca, R.M., 2001. Constraints from 210 Pb and 7 Be on wet
1292 deposition and transport in a global three-dimensional chemical tracer model driven by
1293 assimilated meteorological fields. Journal of Geophysical Research 106, 12109e12128.

1294 McGregor, J. L.: C-CAM Geometric Aspects and Dynamical Formulation, Tech. Rep. 70,
1295 CSIRO Atmospheric Research, Aspendale, Victoria, 2005.

1296 MACC VAL report, Validation report of the MACC reanalysis of global atmospheric
1297 composition Period, 2003-
1298 2011.http://www.copernicusatmosphere.eu/documents/maccii/deliverables/val/MACCII_VA
1299 L_DEL_D_83.4_REAreport02_20130207.pdf, 2013

1300 Mann, G. W., Carslaw, K. S., Spracklen, D. V., Ridley, D. A., Manktelow, P. T.,
1301 Chipperfield, M. P., Pickering, S. J., and Johnson, C. E.: Description and evaluation of
1302 GLOMAP-mode: a modal global aerosol microphysics model for the UKCA composition-
1303 climate model, Geosci. Model Dev., 3, 519-551, doi:10.5194/gmd-3-519-2010, 20103-651-
1304 2010, 2010.

1305 Marenco, A., Thouret, V., Ńeďelec, P., Smit, H. G., Helten, M., Kley, D., Karcher, F., Simon,
1306 P., Law, K., Pyle, J., Poschmann, G., Von Wrede, R., Hume, C., and Cook, T.: Measurement
1307 of ozone and water vapour by Airbus in-service air-craft: The MOZAIC airborne programme,
1308 an overview, J. Geophys. Res., 103, 25631–25642, 1998.

1309 Mari, C., Jacob, D. J., and Bechtold, P.: Transport and scavenging of soluble gases in a deep
1310 convective cloud, J. Geophys. Res., 105, 22 255-22 267, 2000.

1311 Matsumi, Y., Comes, F. J., Hancock, G., Hofzumahus, A., Hynes, A. J., Kawasaki, M., and
1312 Ravishankara, A. R.: Quantum yields for the production of O(1D) in the ultraviolet photolysis
1313 of ozone: recommendation based on evaluation of laboratory data, J. Geophys. Res., 107,
1314 4024, doi:10.1029/2001JD000510, 2002.

1315 Meijer, E.W., P. F. J. van Velthoven, D. W. Brunner, H. Huntrieser and H. Kelder:
1316 Improvement and evaluation of the parameterization of nitrogen oxide production by
1317 lightning, Physics and Chemistry of the Earth, Part C, Volume 26, Issue 8, Pages 577-583,
1318 2001.

1319 Ménard , R. et al. ,Coupled chemical-dynamical data assimilation, Final Report, ESA/ESTEC.
1320 2007.

1321 Metzger, S., F. Dentener, S. Pandis, and J. Lelieveld, Gas/aerosol partitioning, 1, A
1322 computationally efficient model, J. Geophys. Res., 107(D16), doi:10.1029/2001JD001102,
1323 2002a.

1324 Metzger, S., Dentener, F., Krol, M. C., Jeuken, A., and Lelieveld, J.: Gas/aerosol partitioning
1325 2. Global modeling results, J. Geophys. Res., 107(D16), 4313, doi:10.1029/2001JD001103,
1326 2002b.

1327 Michou M., P. Laville, D. Serça, A. Fotiadi, P. Bouchou and V.-H. Peuch, Measured and
1328 modeled dry deposition velocities over the ESCOMPTE area, Atmos. Res., 74 (1-4), 89-116,
1329 2004.

1330 Monks, S. A., Arnold, S. R., Emmons, L. K., Law, K. S., Turquety, S., Duncan, B. N.,
1331 Flemming, J., Huijnen, V., Tilmes, S., Langner, J., Mao, J., Long, Y., Thomas, J. L.,
1332 Steenrod, S. D., Raut, J. C., Wilson, C., Chipperfield, M. P., Schlager, H., and Ancellet, G.:
1333 Multi-model study of chemical and physical controls on transport of anthropogenic and
1334 biomass burning pollution to the Arctic, Atmos. Chem. Phys. Discuss., 14, 25281-25350,
1335 doi:10.5194/acpd-14-25281-2014, 2014.

1336 Morcrette, J.-J., Boucher, O., Jones, L., Salmond, D. , Bechtold, P., Beljaars, A., Benedetti,
1337 A., Bonet, A., Kaiser, J. W., Razinger, M., Schulz, M. , Serrar, S. , Simmons, A. J., Sofiev,
1338 M., Suttie, M., Tompkins, A. M. and Untch, A.: Aerosol analysis and forecast in the ECMWF
1339 Integrated Forecast System. Part I: Forward modelling, J. Geophys. Res., 2009.

1340 Morgenstern, O., Braesicke, P., O'Connor, F. M., Bushell, A. C., Johnson, C. E., Osprey, S.
1341 M., and Pyle, J. A.: Evaluation of the new UKCA climate-composition model – Part 1: The
1342 stratosphere, Geosci. Model Dev., 2, 43–57, doi:10.5194/gmd-2-43-2009, 2009.

1343 Nedelec, P., Cammas, J.-P., Thouret, V., Athier, G., Cousin, J.-M., Legrand, C., Abonnel, C.,
1344 Lecoeur, F., Cayez, G., and Marizy, C.: An improved infrared carbon monoxide analyser for
1345 routine measurements aboard commercial Airbus aircraft: technical validation and first
1346 scientific results of the MOZAIC III programme, Atmos. Chem. Phys., 3, 1551–1564,
1347 doi:10.5194/acp-3-1551-2003, 2003.

1348 Neu, J. L. and Prather, M. J.: Toward a more physical representation of precipitation
1349 scavenging in global chemistry models: cloud overlap and ice physics and their impact on
1350 tropospheric ozone, Atmos. Chem. Phys., 12, 3289-3310, doi:10.5194/acp-12-3289-2012,
1351 2012.

1352 O'Connor, F. M., Johnson, C. E., Morgenstern, O., Abraham, N. L., Braesicke, P., Dalvi, M.,
1353 Folberth, G. A., Sanderson, M. G., Telford, P. J., Voulgarakis, A., Young, P. J., Zeng, G.,
1354 Collins, W. J., and Pyle, J. A.: Evaluation of the new UKCA climate-composition model –
1355 Part 2: The Troposphere, Geosci. Model Dev., 7, 41-91, doi:10.5194/gmd-7-41-2014, 2014.

1356 Olivier J., J. Peters, C. Granier, G. Petron, J.F. Muller, and S. Wallens: Present and future
1357 surface emissions of atmospheric compounds, POET report #2, EU project EVK2-1999-
1358 00011, 2003

1359 Ordóñez, C., Elguindi, N., Stein, O., Huijnen, V., Flemming, J., Inness, A., Flentje, H.,
1360 Katragkou, E., Moinat, P., Peuch, V.-H., Segers, A., Thouret, V., Athier, G., van Weele, M.,
1361 Zerefos, C. S., Cammas, J.-P., and Schultz, M. G.: Global model simulations of air pollution
1362 during the 2003 European heat wave, Atmos. Chem. Phys., 10, 789-815, doi:10.5194/acp-10-
1363 789-2010, 2010.

1364 Ott, L. E., K. E. Pickering, G. L. Stenchikov, D. J. Allen, A. J. DeCaria, B. Ridley, R.-F. Lin,
1365 S. Lang, and W.-K. Tao (2010), Production of lightning NOx and its vertical distribution

1366 calculated from three-dimensional cloud-scale chemical transport model simulations, J.
1367 Geophys. Res., 115, D04301, doi:10.1029/2009JD011880.

1368 Pickering, K. E., Y. Wang, W.-K. Tao, C. Price, and J.-F. Müller: Vertical distributions of
1369 lightning NOx for use in regional and global chemical transport models, J. Geophys. Res.,
1370 103, 31,203 – 31,216, doi:10.1029/98JD0265. 1998.

1371 Pozzoli L., Bey, I., Rast, J. S., Schultz, M. G., Stier, P., and Feichter, J.: Trace gas and aerosol
1372 interactions in the fully coupled model of aerosol-chemistry-climate ECHAM5-HAMMOZ,
1373 PART I: Model description and insights from the spring 2001 TRACE-P experiment, J.
1374 Geophys. Res., 113 , 2008.

1375 Prather, M., Ehhalt, D., et al.: Atmospheric chemistry and greenhouse gases, in: Climate
1376 Change 2001: The Scientific Basis, edited by: Houghton, J. T., Ding, Y., Griggs, D. J., et al.,
1377 239–287, Cambridge University Press, Cambridge, UK, 2001.

1378 Prather, M. J., Holmes, C. D., and Hsu, J.: Reactive greenhouse gas scenarios: Systematic
1379 exploration of uncertainties and the role of atmospheric chemistry, Geophys. Res. Lett., 39,
1380 L09803,doi:10.1029/2012GL051440, 2012.

1381 Price, C., and Rind, D.: A simple lightning parameterization for calculating global lightning
1382 distributions, J. Geophys. Res., 9 7, 9919-9933, 1992.

1383 Price, C., and Rind, D.: What determinest he cloud-to-ground fraction in thunderstorms?
1384 Geophys Res. Lett., 20, 463-466, 1993.

1385 Price, C., J. Penner, and M. Prather: NOx from lightning 1. Global distributions based on
1386 lightning physics, J. Geophys. Res., 102, 5929–5941, doi:10.1029/96JD03504, 1997.

1387 Rast, S., Schultz, M.G. , Bey, I., van Noije, T. , Aghedo, A.M. , Brasseur, G.P., Diehl, T.,
1388 Esch, M., Ganzeveld, L., Kirchner, I., Kornblueh, L., Rhodin, A. , Röckner, E. , Schmidt, H. ,
1389 Schröder, S., Schulzweida, U., Stier, P., Thomas, K., Walters, S.: Evaluation of the
1390 tropospheric chemistry general circulation model ECHAM5–MOZ and its application to the
1391 analysis of the chemical composition of the troposphere with an emphasis on the late RETRO
1392 period 1990–2000, Reports on Earth-System Science, 114, Max-Planck Institut fuer
1393 Meteorologie, Hamburg, 2014.

1394 Redler, R., Valcke, S. and Ritzdorf, H.: OASIS4 - A Coupling Software for Next Generation
1395 Earth System Modelling, Geoscience Model Development, 3, 87 - 104, DOI:10.5194/gmd-3-
1396 87-2010.

1397 Richter, A., Burrows, J. P., Nüß, H., Granier, C, Niemeier, U., Increase in tropospheric
1398 nitrogen dioxide over China observed from space, Nature, 437, 129-132, doi:
1399 10.1038/nature04092, 2005.

1400 Sander, R., Compilation of Henry's Law Constants for Inorganic and Organic Species of
1401 Potential Importance in Environmental Chemistry, MPI for Chemistry Mainz, Germany,
1402 1999, http://www.henrys-law.org/henry.pdf

1403 Sander, S. P., Friedl, R. R., Golden, D. M., Kurylo, M. J., Moortgat, G. K., Keller-Rudek, H.,
1404 Wine, P. H., Ravishankara, A. R., Kolb, C. E., Molina, M. J., Finlayson-Pitts, B. J., Huie, R.
1405 E., and Orkin, V. L: Chemical Kinetics and Photochemical Data for Use in Atmospheric
1406 Studies, Evaluation Number 15, JPL Publication 06-02, Jet Propulsion Laboratory, Pasadena,
1407 Calif., 2006.

1408 Sander, S. P., Abbatt, J. R., Burkholder, J. B., Friedl, R. R., Golden, D. M., Huie, R. E., Kolb,
1409 C. E., Kurylo, G., Moortgat, K., Orkin, V. L. and Wine, P. H.: Chemical kinetics and
1410 Photochemical Data for Use in Atmospheric studies, Evaluation No.17, JPL Publication 10-6,
1411 Jet Propulsion Laboratory, Pasadena, 2011.

1412 Savage, N. H., Agnew, P., Davis, L. S., Ordóñez, C., Thorpe, R., Johnson, C. E., O'Connor, F.
1413 M., and Dalvi, M.: Air quality modelling using the Met Office Unified Model (AQUM OS24-
1414 26): model description and initial evaluation, Geosci. Model Dev., 6, 353-372,
1415 doi:10.5194/gmd-6-353-2013, 2013.

1416 Schumann, U., and H. Huntrieser: The global lightning-induced nitrogen oxides source,
1417 Atmos. Chem. Phys., 7, 3823–3907, 2007.

1418 Seinfeld J. H. and Pandis S. N., Atmospheric Chemistry and Physics: From Air Pollution to
1419 Climate Change, 1st edition, J. Wiley, New York, 1998.

1420 Shindell, D.T., G. Faluvegi, D.S. Stevenson, M.C. Krol, L.K. Emmons, J.-F. Lamarque, G.
1421 Pétron, F.J. Dentener, K. Ellingsen, M.G. Schultz, O. Wild, M. Amann, C.S. Atherton, D.J.
1422 Bergmann, I. Bey, T. Butler, J. Cofala, W.J. Collins, R.G. Derwent, R.M. Doherty, J. Drevet,
1423 H.J. Eskes, A.M. Fiore, M. Gauss, D.A. Hauglustaine, L.W. Horowitz, I.S.A. Isaksen, M.G.
1424 Lawrence, V. Montanaro, J.-F. Müller, G. Pitari, M.J. Prather, J.A. Pyle, S. Rast, J.M.

1425 Rodriguez, M.G. Sanderson, N.H. Savage, S.E. Strahan, K. Sudo, S. Szopa, N. Unger, T.P.C.
1426 van Noije, and G. Zeng: Multi-model simulations of carbon monoxide: Comparison with
1427 observations and projected near-future changes. J. Geophys. Res., 111, D19306,
1428 doi:10.1029/2006JD007100, 2006.

1429 Slingo, A.: A GCM parameterization for the shortwave radiative properties of water clouds. J.
1430 Atmos. Sci., 46, 1419–1427, 1989.

1431 Smithson, P. A., IPCC, 2001: climate change 2001: the scientific basis. Contribution of
1432 Working Group 1 to the Third Assessment Report of the Intergovernmental Panel on Climate
1433 Change, edited by J. T. Houghton, Y. Ding, D. J. Griggs, M. Noguer, P. J. van der Linden, X.
1434 Dai, K. Maskell and C. A. Johnson (eds). Cambridge University Press, Cambridge, UK, and
1435 New York, USA, Int. J. Climatol., 22: 1144. doi: 10.1002/joc.763, 2002.

1436 Steil, B., Dameris, M., Brühl, C., Crutzen, P. J., Grewe, V., Ponater, M., and Sausen, R.:
1437 Development of a chemistry module for GCMs: first results of a multiannual integration,
1438 Ann. Geophys., 16, 205-228, doi:10.1007/s00585-998-0205-8, 1998.

1439 Stein, O., Flemming, J., Inness, A., Kaiser, J.W., Schultz, M.G. , Global reactive gases
1440 forecasts and reanalysis in the MACC project, Journal of Integrative Environmental Sciences,
1441 9, Iss. sup1, 57-70, doi:10.1080/1943815X.2012.696545, 2012.

1442 Stein, O., Schultz, M. G., Bouarar, I., Clark, H., Huijnen, V., Gaudel, A., George, M., and
1443 Clerbaux, C.: On the wintertime low bias of Northern Hemisphere carbon monoxide in global
1444 model studies, Atmos. Chem. Phys. Discuss., 14, 245-301, doi:10.5194/acpd-14-245-2014,
1445 2014.

1446 Steinbrecht, W., Shwartz, R., and Claude, H.: New pump correction for the Brewer-Mast
1447 ozonesonde: Determination from experiment and instrument intercomparisons, J. Atmos.
1448 Ocean. Tech.15, 144–156, 1998.

1449 Stevenson, D. S., et al. (2006), Multimodel ensemble simulations of present-day and near-
1450 future tropospheric ozone, J. Geophys. Res., 111, D08301, doi:10.1029/2005JD006338.

1451 Temperton, C., Hortal, M. and Simmons, A.: A two-time-level semi-Lagrangian global
1452 spectral model, QJR, 127, 111-127, 2001.

1453 Tiedtke, M. A: comprehensive mass flux scheme for cumulus parameterization in large-scale
1454 models. Mon. Weather. Rev., 117(8):1779-1800, 1989.

Tilmes, S., Lamarque, J.-F., Emmons, L. K., Conley, A., Schultz, M. G., Saunois, M., Thouret, V., Thompson, A. M., Oltmans, S. J., Johnson, B., and Tarasick, D.: Technical Note: Ozonesonde climatology between 1995 and 2011: description, evaluation and applications, Atmos. Chem. Phys., 12, 7475-7497, doi:10.5194/acp-12-7475-2012, 2012.

Wesely, M.L.: Parameterization of Surface Resistances to Gaseous Dry Deposition in Regional-Scale Numerical Models. Atmos. Environ., 23, 1293-1304, 1989.

Val Martin, M., Heald, C. L. and Arnold, S. R.: Coupling dry deposition to vegetation phenology in the Community Earth System Model: Implications for the simulation of surface O3, Geophys. Res. Lett., 41, 2988–2996, doi:10.1002/2014GL059651., 2014van Noije, T. P. C., Le Sager, P., Segers, A. J., van Velthoven, P. F. J., Krol, M. C., Hazeleger, W., Williams, A. G., and Chambers, S. D.: Simulation of tropospheric chemistry and aerosols with the climate model EC-Earth, Geosci. Model Dev., 7, 2435-2475, doi:10.5194/gmd-7-2435-2014, 2014.

von Blohn, N., Diehl, K., Mitra, S. K., and Borrmann, S.: Wind tunnel experiments on the retention of trace gases during riming: nitric acid, hydrochloric acid, and hydrogen peroxide, Atmos. Chem. Phys., 11, 11569-11579, doi:10.5194/acp-11-11569-2011, 2011.

Voulgarakis, A., Naik, V., Lamarque, J.-F., Shindell, D. T., Young, P. J., Prather, M. J., Wild, O., Field, R. D., Bergmann, D., Cameron-Smith, P., Cionni, I., Collins, W. J., Dalsøren, S. B., Doherty, R. M., Eyring, V., Faluvegi, G., Folberth, G. A., Horowitz, L. W., Josse, B., MacKenzie, I. A., Nagashima, T., Plummer, D. A., Righi, M., Rumbold, S. T., Stevenson, D. S., Strode, S. A., Sudo, K., Szopa, S., and Zeng, G.: Analysis of present day and future OH and methane lifetime in the ACCMIP simulations, Atmos. Chem. Phys., 13, 2563-2587, doi:10.5194/acp-13-2563-2013, 2013.

Vrekoussis, M., Wittrock, F., Richter, A., and Burrows, J. P.: GOME-2 observations of oxygenated VOCs: what can we learn from the ratio glyoxal to formaldehyde on a global scale?, Atmos. Chem. Phys., 10, 10145-10160, doi:10.5194/acp-10-10145-2010, 2010.

Williams, J. E., Strunk, A., Huijnen, V., and van Weele, M.: The application of the Modified Band Approach for the calculation of on-line photodissociation rate constants in TM5: implications for oxidative capacity, Geosci. Model Dev., 5, 15-35, doi:10.5194/gmd-5-15-2012, 2012.

Williams, J. E., van Velthoven, P. F. J., and Brenninkmeijer, C. A. M.: Quantifying the uncertainty in simulating global tropospheric composition due to the variability in global emission estimates of Biogenic Volatile Organic 2857-2013, 2013.

Wittrock, F., A. Richter, H. Oetjen, J. P. Burrows, M. Kanakidou, S. Myriokefalitakis, R. Volkamer, S. Beirle, U. Platt, and T. Wagner, Simultaneous global observations of glyoxal and formaldehyde from space, Geophys. Res. Lett., 33, L16804, doi:10.1029/2006GL026310, 2006Compounds, Atmos. Chem. Phys., 13, 2857-2891, doi:10.5194/acp-13-2857-2013, 2013.

Yarwood, G., Rao, S., Yocke, M., and Whitten, G.: Updates to the carbon bond chemical mechanism: CB05. Final report to the US EPA, EPA Report Number: RT-0400675, available at: www.camx.com, last access: 1 July 2014, 2005.

WMO (2007), WMO Global Atmosphere Watch (GAW) Strategic Plan: 2008 – 2015. World Meteorological Organization, Geneva, Switzerland, 2007.

Young, P. J., Archibald, A. T., Bowman, K. W., Lamarque, J.-F., Naik, V., Stevenson, D. S., Tilmes, S., Voulgarakis, A., Wild, O., Bergmann, D., Cameron-Smith, P., Cionni, I., Collins, W. J., Dalsøren, S. B., Doherty, R. M., Eyring, V., Faluvegi, G., Horowitz, L. W., Josse, B., Lee, Y. H., MacKenzie, I. A., Nagashima, T., Plummer, D. A., Righi, M., Rumbold, S. T., Skeie, R. B., Shindell, D. T., Strode, S. A., Sudo, K., Szopa, S., and Zeng, G.: Pre-industrial to end 21st century projections of tropospheric ozone from the Atmospheric Chemistry and Climate Model Intercomparison Project (ACCMIP), Atmos. Chem. Phys., 13, 2063-2090, doi:10.5194/acp-13-2063-2013, 2013.

Zaveri, R. A. and Peters, L. K.: A new lumped structure photochemical mechanism for large-scale applications, J. Geophys. Res., 104, 30387–30415, doi:10.1029/1999JD900876, 1999.

Zdunkowski, W. G., Welsch, R. M., and Kord, G. J.: An investigation of the structure of typical 2-stream methods for the calculation of solar fluxes and heating rates in clouds, Contrib. Atmos. Phys., 53, 215–238, 1980.

Zhang, L., Brook, J. R., and Vet, R.: A revised parameterization for gaseous dry deposition in air-quality models, Atmos. Chem. Phys., 3, 2067-2082, doi:10.5194/acp-3-2067-2003, 2003.

Zhang, Y.: On-line coupled meteorology and chemistry models: history, current status, and outlook, Atmos. Chem. Phys, 8, 2895-2032, 2008.

Zhang, Y., Karamchandani, P. , Glotfelty, T., Streets, D. G., Grell, G. , Nenes, A. , Yu, F. and Bennartz, R.: Development and initial application of the global-through-urban weather research and forecasting model with chemistry (GU-WRF/Chem), J. Geophys. Res., 117, D20206, doi:10.1029/2012JD017966, 2012.

Table 1 Annual emissions from anthropogenic, biogenic and natural sources and biomass burning for 2008 in Tg for a C-IFS (CB05) run at T255 resolution. Anthropogenic NO emissions contain a contribution of 1.8 Tg aircraft emissions and 12.3 Tg (5.7 Tg N) lightning emissions (LiNO) is added in the biomass burning columns.

Species	Anthropogenic	Biogenic and natural	Biomass burning
CO	584	96	328
NO	70 + 1.8	10	9.2 + 12.3 (LiNO)
HCHO	3.4	4.0	4.9
CH_3OH	2.2	159	8.5
C_2H_6	3.4	1.1	2.3
C_2H_5OH	3.1	0	0
C_2H_4	7.7	18	4.3
C_3H_8	4.0	1.3	1.2
C_3H_6	3.5	7.6	2.5
Parafins (Tg C)	31	18	1.7
Olefines (Tg C)	2.4	0	0.7
Aldehydes (Tg C)	1.1	6.1	2.1
CH_3COCH_3	1.3	28	2.4
Isoprene	0	523	0
Terpenes	0	97	0
SO_2	98	9	2.2
DMS	0	38	0.2
NH_3	40	11	6.2

1524 Table 2 Ozone sondes sites used in the evaluation for different regions

Region	Area S/W/N/E	Stations (Number of observations)
Europe	35°N/20°W/60°N/40°E	Barajas (52), DeBilt (57), Hohenpeissenberg (126), Legionowo (48), Lindenberg (52), Observatoire de Haute-Provence (46), Payerne (158), Prague (49), Uccle (142) and Valentia Observatory (49)
North America:	30°N/135°W/60°N/60°W	Boulder (65), Bratts Lake (61), Churchill (61), Egbert (29), Goose Bay (47), Kelowna (72), Stony Plain (77), Wallops (51), Yarmouth (60), Narragansett (7) and Trinidad Head (35)
Arctic:	60°N/180°W/90°N/180°E	Alert (52), Eureka (83), Keflavik (8), Lerwick (49), Ny-Aalesund (77), Resolute (63), Scoresbysund (54), Sodankyla (63), Summit (81) and Thule(15)
Tropics	20°S/180°W/20°N/180°E	Alajuela (47), Ascension Island (32), Hilo (47), Kuala Lumpur (24), Nairobi (39), Natal (48), Paramaribo (35), Poona (13), Samoa (33), San Cristobal (28), Suva (28), Thiruvananthapuram (12) and Watukosek (19)
East Asia	15°N/100°E/45°N/142°E	Hong Kong Observatory (49), Naha (37), Sapporo (42) and Tateno Tsukuba (49)
Antarctic	90°S/180°W/60°S/180°E	Davis (24), Dumont d'Urville (38), Maitri (9), Marambio (66), Neumayer (72), South Pole (63), Syowa(41) and McMurdo (18)

1525

1526 Table 3 Computational cost (BU) of a 24 h forecasts of different horizontal model resolutions
1527 (60 levels) and chemistry schemes of C-IFS, IFS-MOZART and IFS, *not fully optimised.

Resolution	IFS-MOZART	C-IFS (MOZART)*	C-IFS (MOCAGE)*	C-IFS (CB05)	IFS
T159	205	56	147	20	6
T255	1200	-	-	55	12
T511	-	-	-	700	125

1528
1529

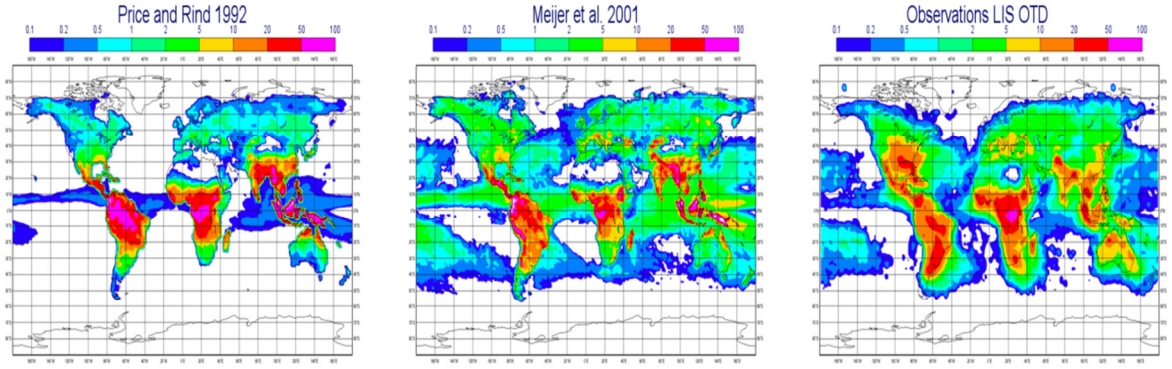

1530

1531

1532 Figure 1 Flash density in flashes/(km^2 yr) from the IFS input data using the parameterization
1533 by Price and Rind (1992) (left), Meijer et al. (2001) (middle) and observations from the LIS
1534 OTD data base (right). All fields were scaled to an annual flash density of 46 fl/s.

1535

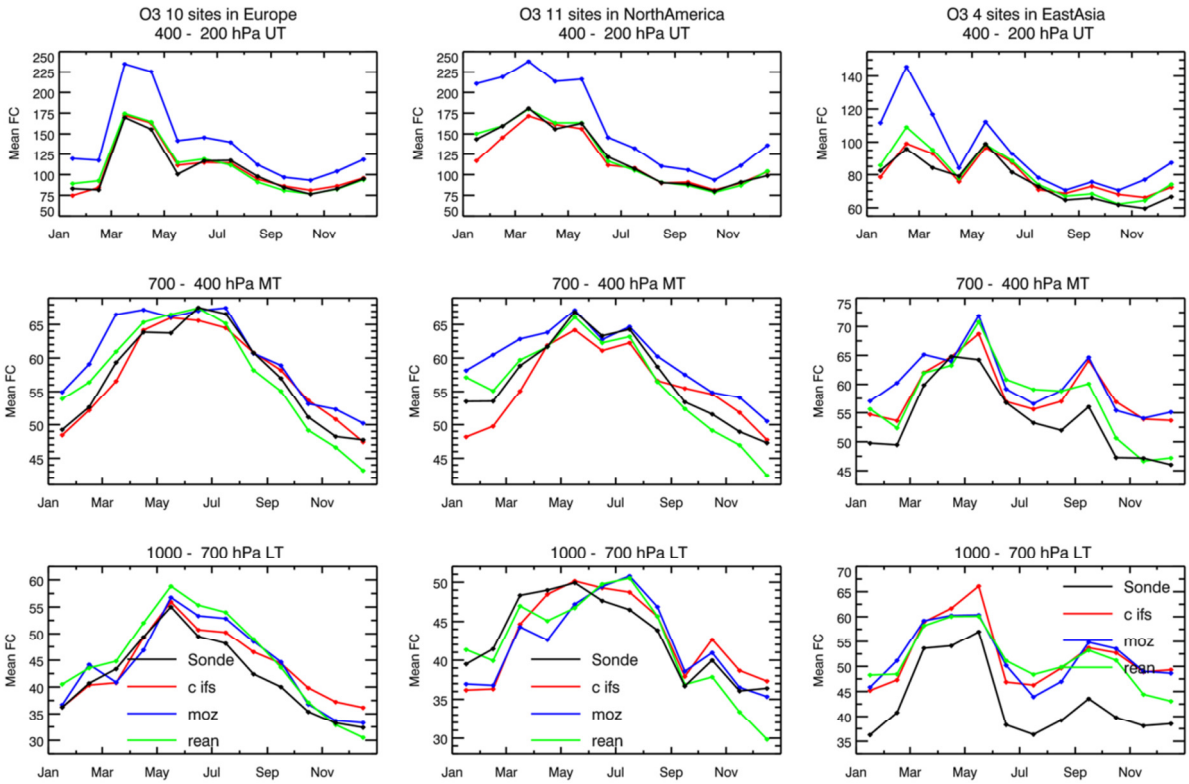

Figure 2 Tropospheric ozone volume mixing ratios (ppb) over Europe (left) and North-America (middle) and East Asia (right) averaged in the pressure range 1000-700 hPa (bottom), 700-400 hPa (middle) and 400-200 hPa (top) observed by ozonesondes (black) and simulated by C-IFS (red), MOZ (blue) and REAN (green) in 2008.

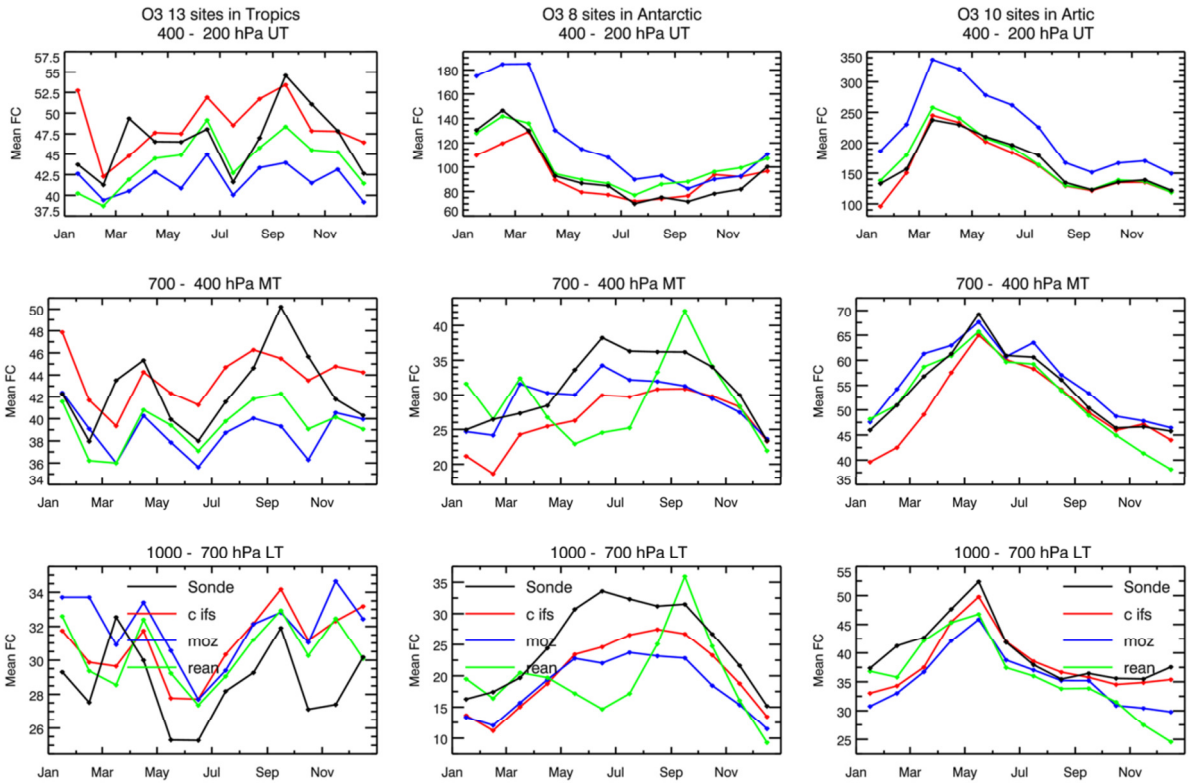

1542

1543 Figure 3 Tropospheric ozone volume mixing ratios (ppb) over the Tropics (left) Antarctica
1544 (middle) and Arctic (right) averaged in the pressure bands 1000-700 hPa (bottom), 700-400
1545 hPa (middle) and 400-200 hPa (top) observed by ozonesondes and simulated by C-IFS (red),
1546 MOZ (blue) and REAN (green) in 2008.

1547

1548

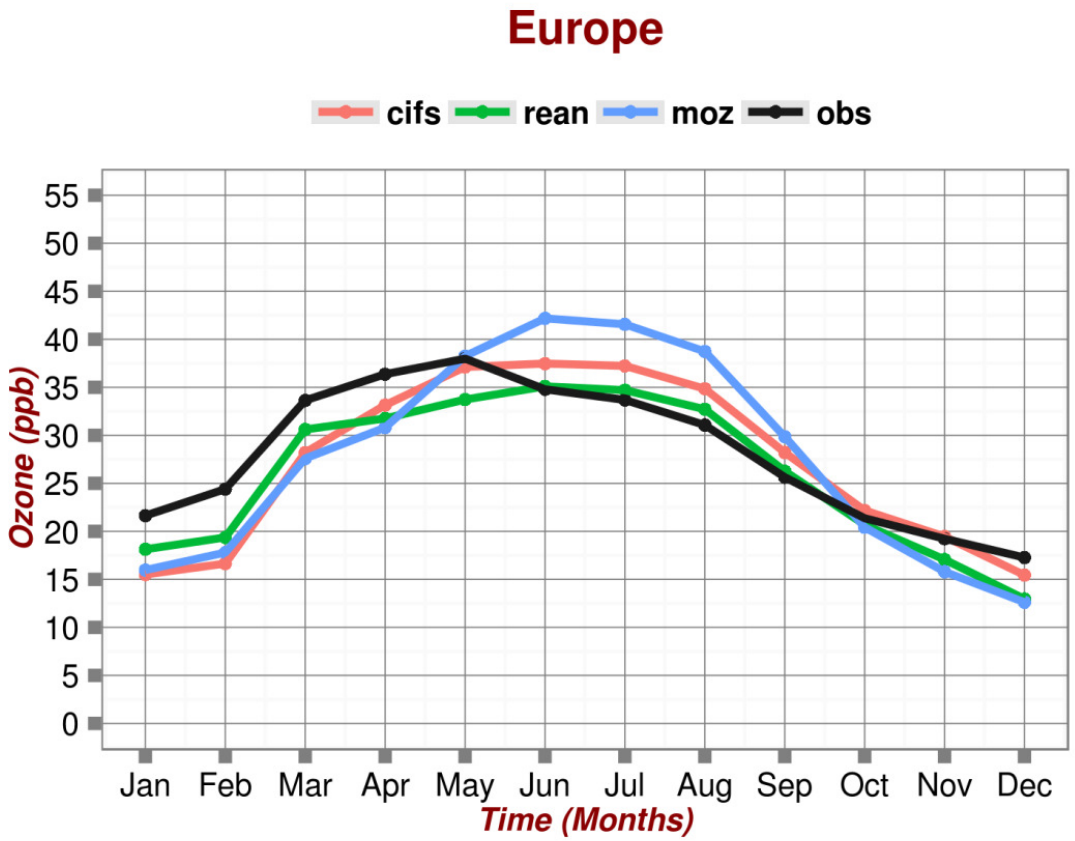

1549

1550 Figure 4 Annual cycle of the mean ozone volume mixing ratios (ppb) at rural sites of the
1551 EMEP and AirBase data base and simulated by C-IFS (red), MOZ (blue) and REAN (green).

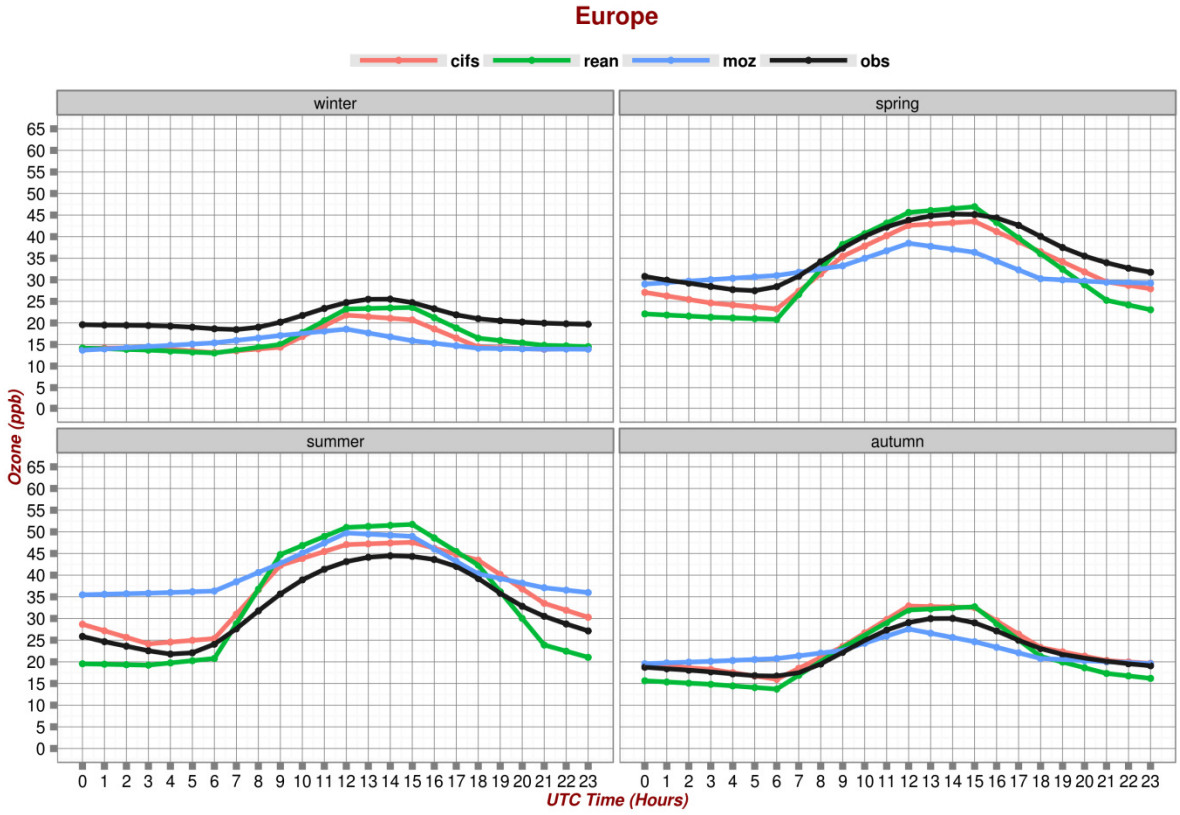

Figure 5 Diurnal cycle of surface ozone volume mixing ratios (ppb) over Europe in winter (top, left), spring (top, right), summer (bottom, left) and autumn (bottom, right) at rural site of the EMEP and AirBase data base and simulated by C-IFS (red), MOZ (blue) and REAN (green).

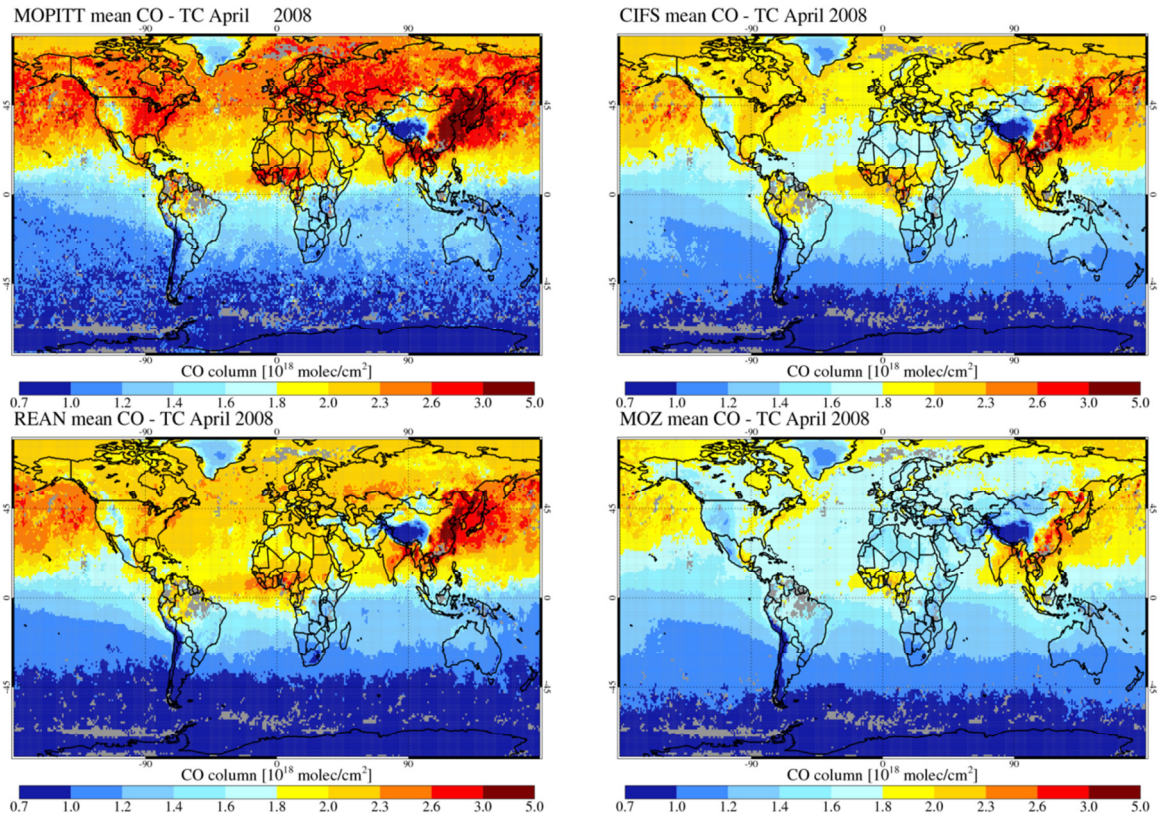

Figure 6 CO total column retrieval (MOPITT V6) for April 2008 (top left) and simulated by C-IFS (top right), MOZ (bottom left) and REAN (bottom right), AK are applied.

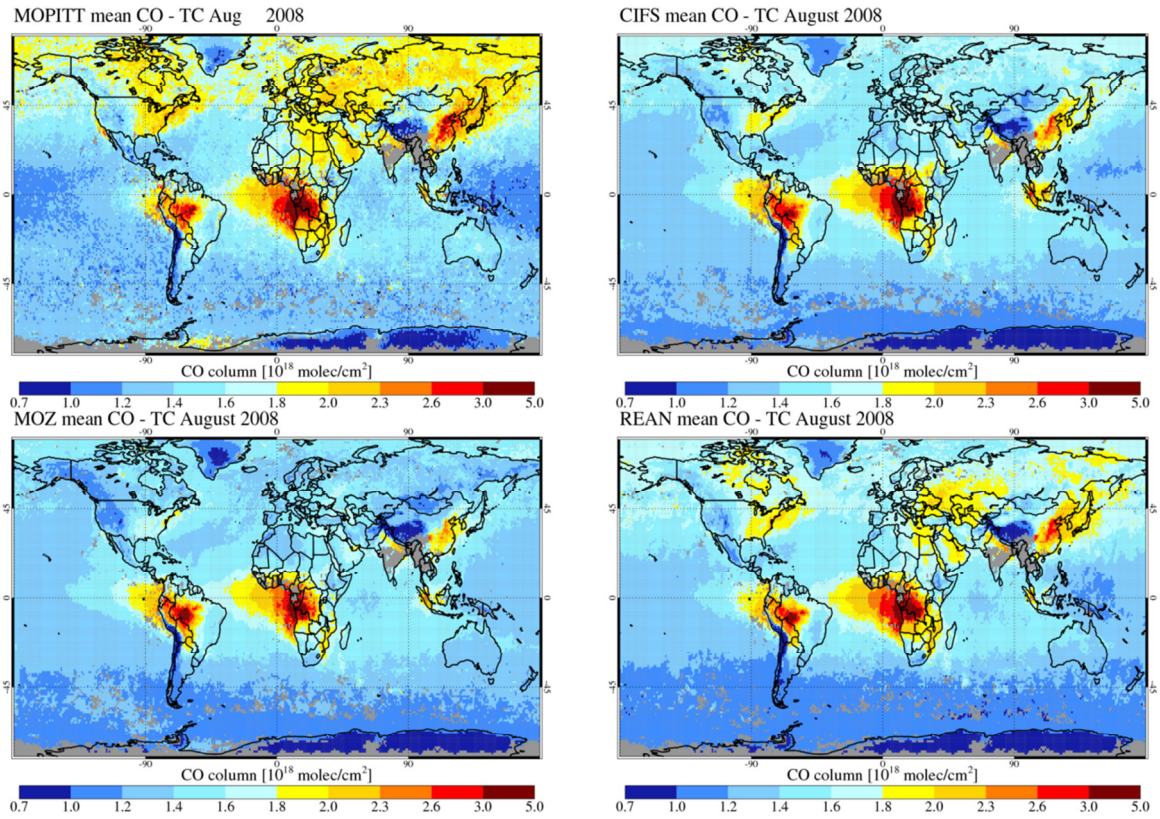

1562

1563 Figure 7 CO total column retrieval (MOPITT V6) for August 2008 (top left) and simulated by

1564 C-IFS (top right), MOZ (bottom right) and REAN (bottom left), AK are applied.

1565

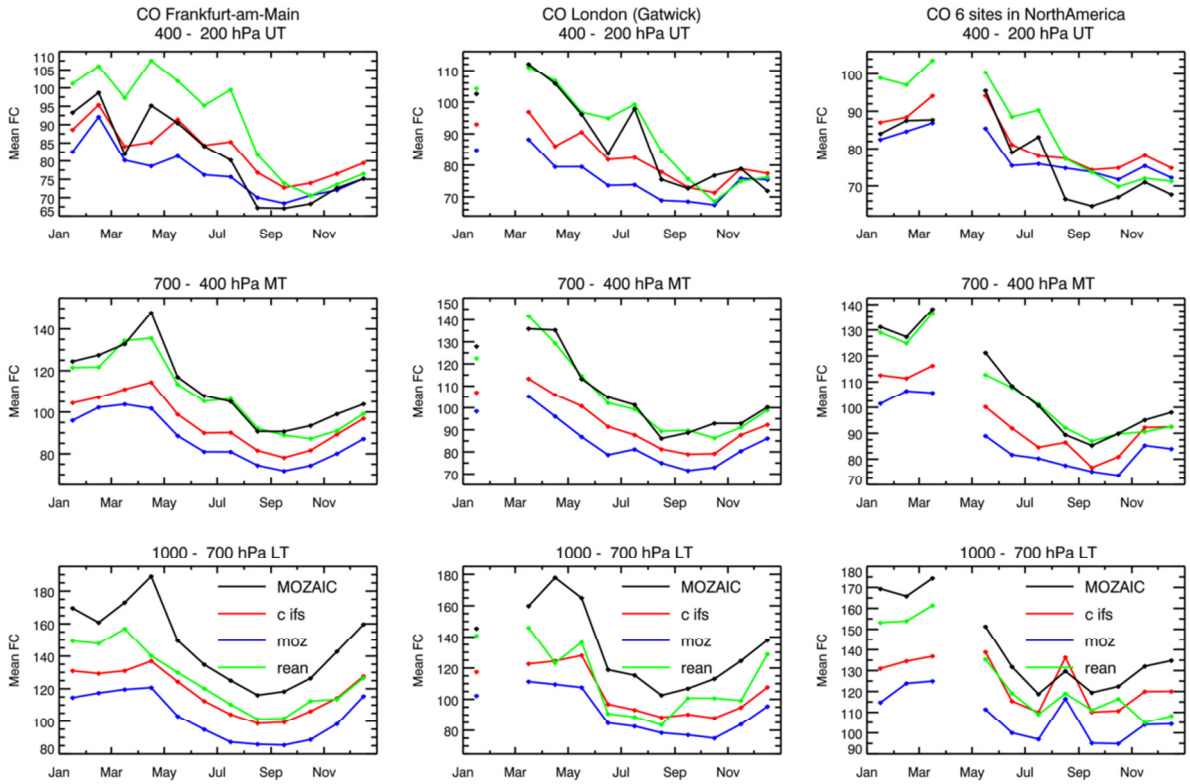

1566

1567 Figure 8 CO volume mixing ratios (ppb) over Frankfurt (left), London (middle) and North
1568 America (left, averaged over 6 airports) averaged in the pressure bands 1000-700 hPa
1569 (bottom), 700-400 hPa (middle) and 400-200 hPa (top) observed by MOZAIC and simulated
1570 by C-IFS (red), MOZ (blue) and REAN (green) in 2008.

1571

1572

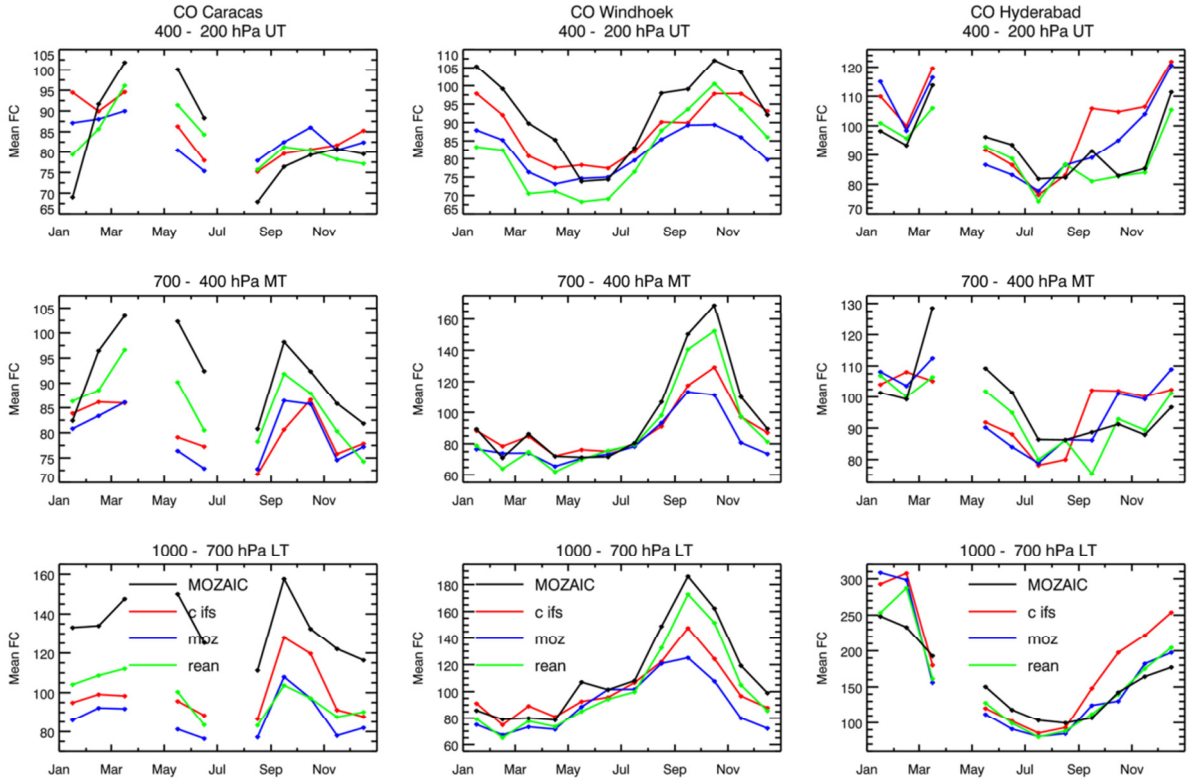

1573

1574 Figure 9 CO volume mixing ratios (ppb) over Caracas (left) Windhoek (middle) and
1575 Hyderabad (right) averaged in the pressure bands 1000-700 hPa (bottom), 700-400 hPa
1576 (middle) and 400-200 hPa (top) observed by MOZAIC, and simulated by C-IFS (red), MOZ
1577 (blue) and REAN (green) in 2008.

1578

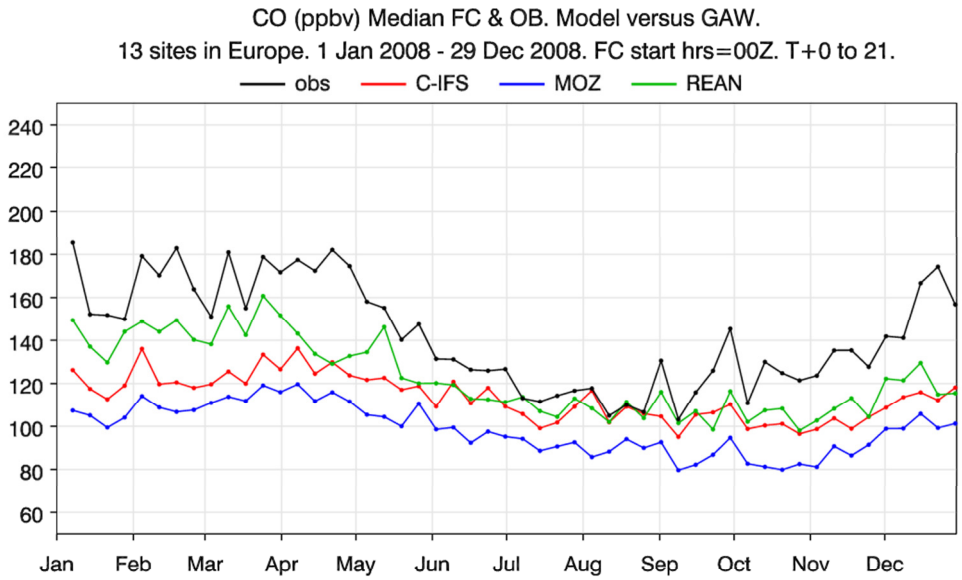

Figure 10 Time series of median of weekly CO surface volume mixing ratios (ppb) in Europe (13 GAW sites) and model results of C-IFS, MOZ and REAN.

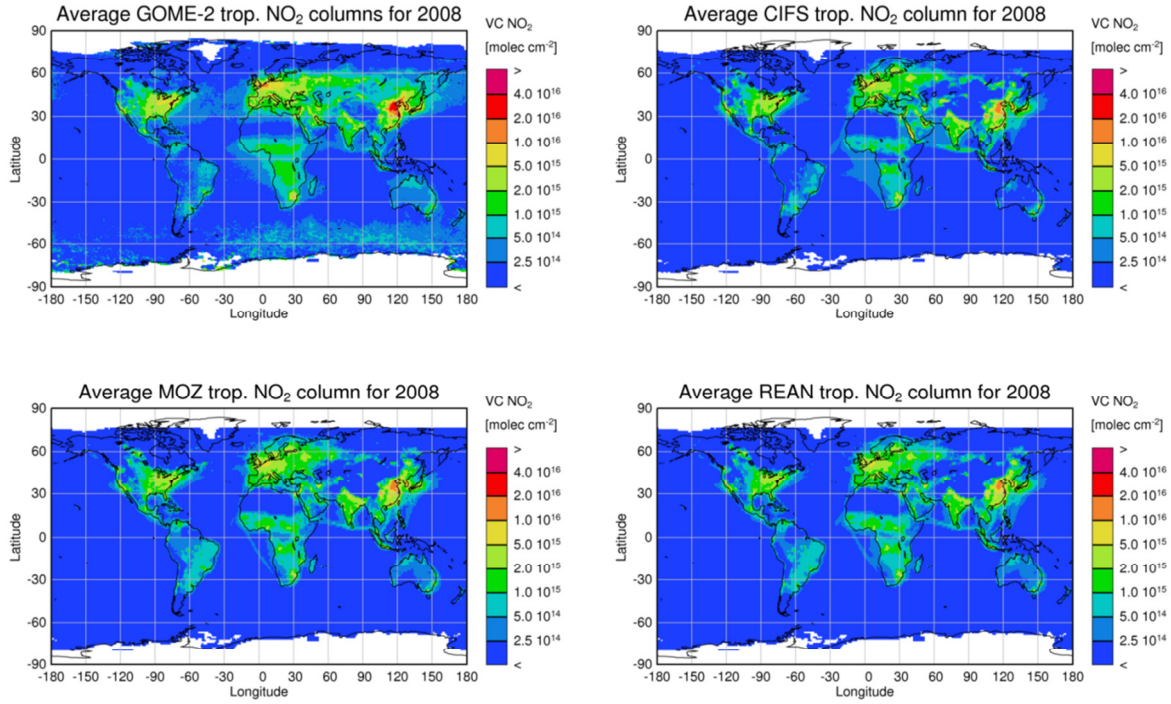

1584

1585

1586 Figure 11 NO_2 tropospheric column retrieval (GOME-2) for 2008 (top left) and by C-IFS (top

1587 right), REAN (bottom right) and MOZ (bottom left)

1588

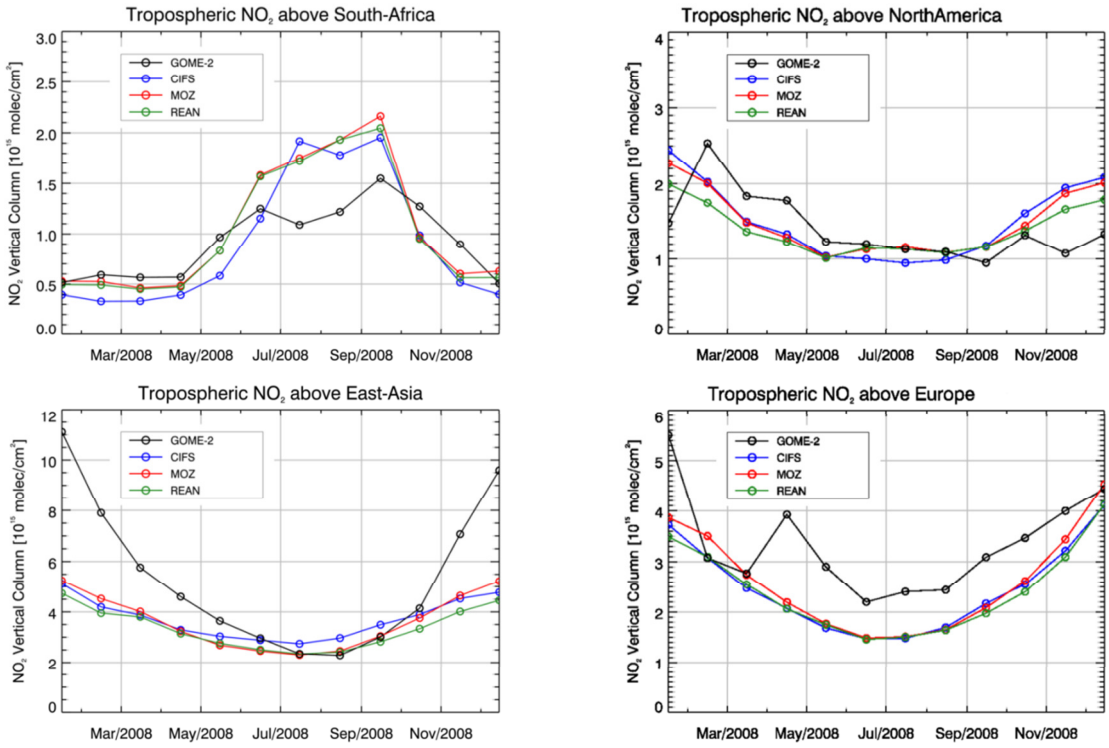

Figure 12 Time series of area-averaged tropospheric NO_2 columns [10^{15} molec cm-2] from GOME-2 compared to model results of C-IFS (CB05) (blue), MOZ (red) and REAN (green) for different regions.

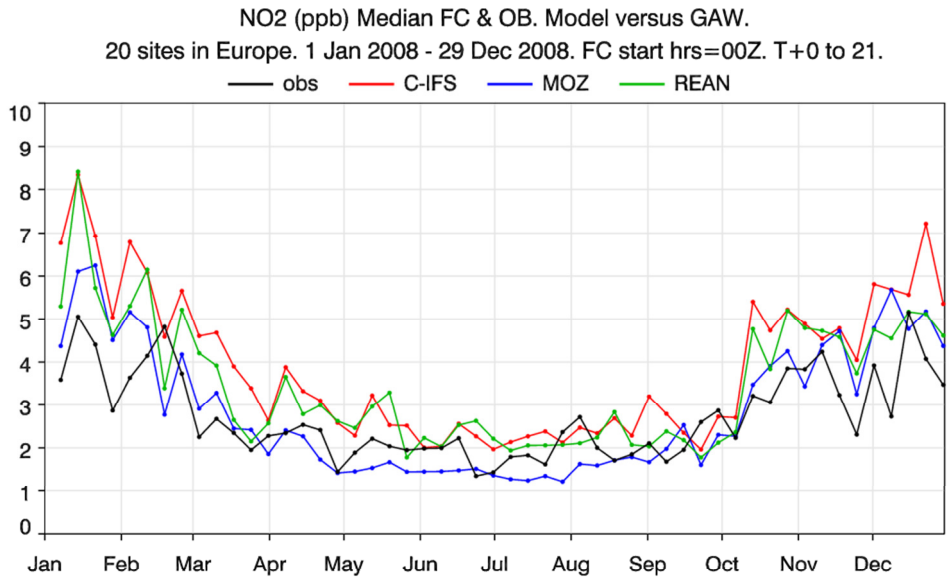

Figure 13 Time series of median of weekly surface NO_2 volume mixing ratios (ppb) in Europe (20 GAW sites) and model results of C-IFS, MOZ and REAN.

1601

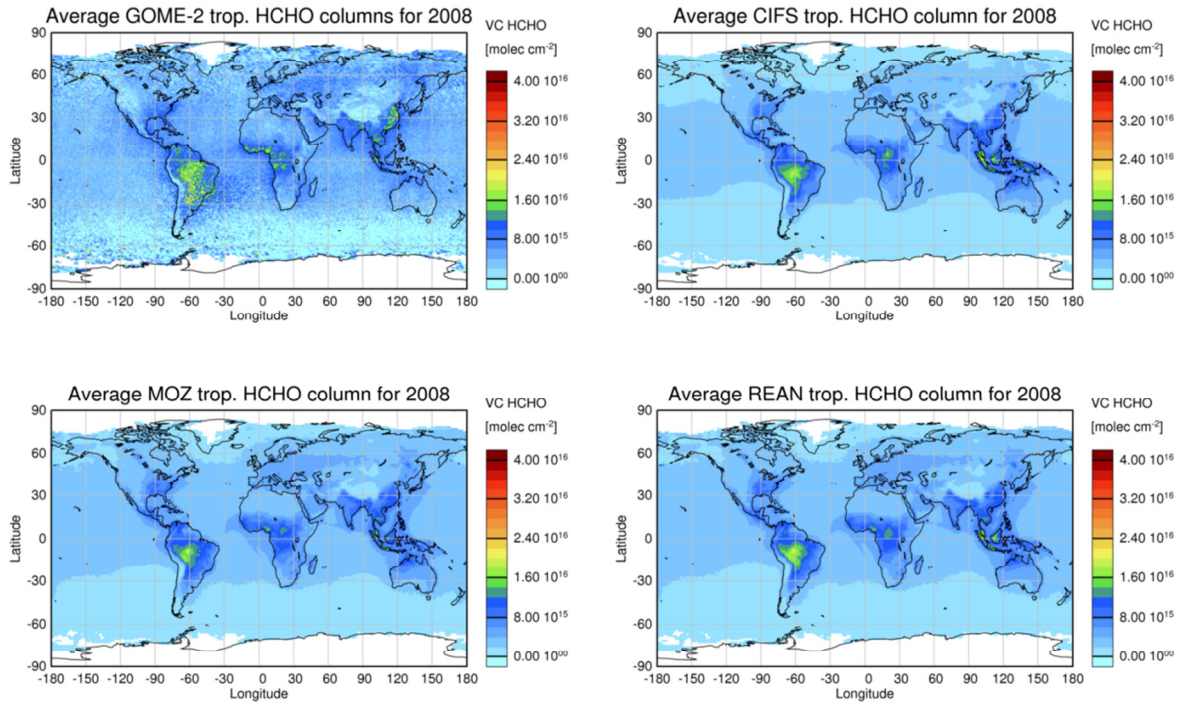

1602

1603 Figure 14 HCHO tropospheric column retrieval (GOME-2) for 2008 (top left) and by C-IFS

1604 (top right), REAN (bottom right) and MOZ (bottom left)

1605

1606

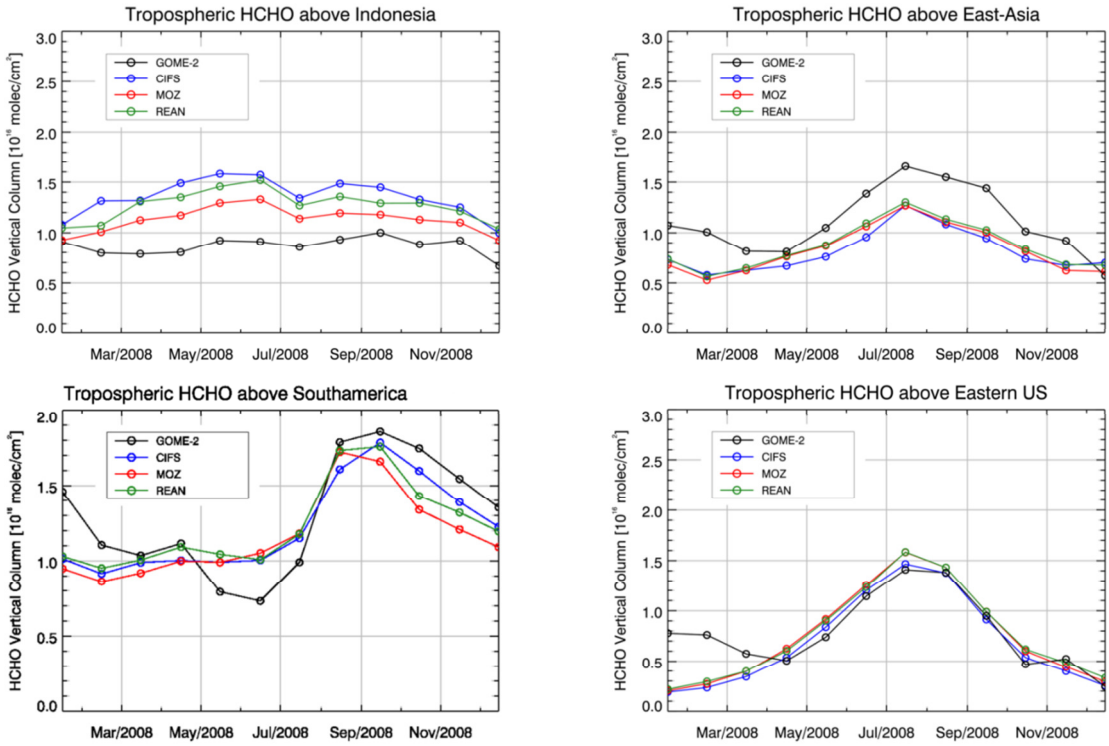

1607

1608

1609 Figure 15 Time series of area-averaged tropospheric HCHO columns [10^{16} molec cm-2] from

1610 GOME-2 compared to model results of C-IFS, MOZ and REAN for different regions.

1611

1612

1613
1614

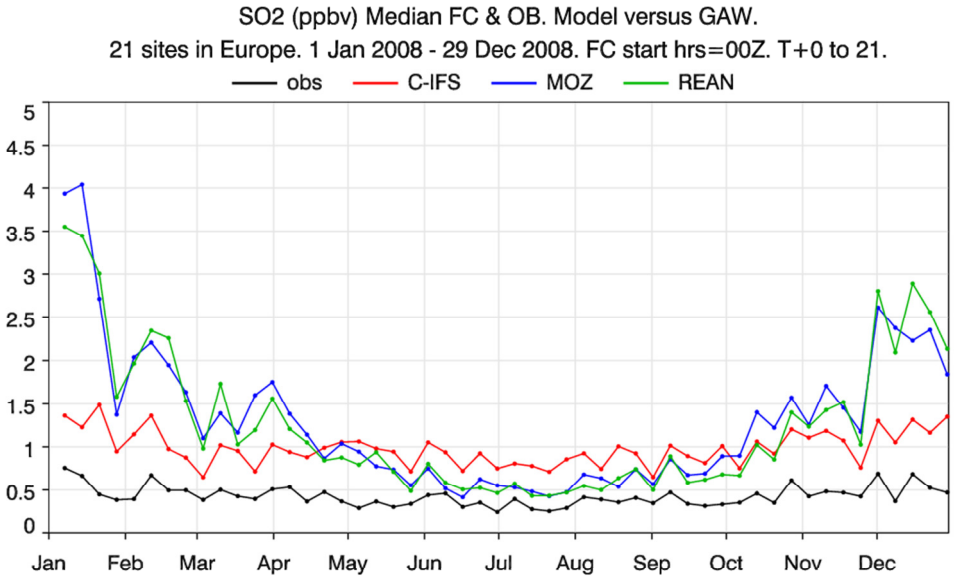

1615
1616 Figure 16 Time series of median of weekly surface SO_2 volume mixing ratios (ppb) in Europe
1617 (21 GAW sites) and model resuls of C-IFS, MOZ and REAN